UNIVERSITY OF CALIFORNIA, SAN DIEGO

Measurement of Landau Damping of Electron Plasma Waves in the Linear and Trapping Regimes

A dissertation submitted in partial satisfaction of the

requirements for the degree Doctor of Philosophy

in Physics

by

James Robert Danielson

Committee in charge:

Professor C. Fred Driscoll, Chairman
Professor William Coles
Professor Daniel Dubin
Professor Thomas O'Neil
Professor George Tynan

2002

The dissertation of James Robert Danielson is approved, and it is acceptable in quality and form for publication on microfilm:

Chairman

University of California, San Diego

2002

This dissertation is dedicated to

my parents,

their love and support allowed me the freedom to dream.

Table of Contents

List of Figures

List of Tables

Acknowledgements

First, I would like to thank my advisor, Fred Driscoll, for constantly challenging me with the simple remark, "make a positive scientific statement." He taught me that small statements of fact can lead us to large volumes of understanding; something I hope to never forget. Further, his influence on my understanding of what the process of doing science should be, will guide me for many years to come.

I also thank Professors Tom O'Neil and Dan Dubin, for their patience with my questions about plasma theory and for always working with me to find the answers. One of the big reasons for my choice of UCSD as a graduate school, was the opportunity to work in the Non-Neutral Plasma Group. The interaction between the experimentalists and the theorists is a fun game which contributes at least as much to the science as the individual work itself. I believe that my experiences and success, although at times not exactly what I expected, has certainly proved to me that my choice was correct.

I also thank JoAnn Christina, whose continual help and support was always there during the most stress-full times. Her understanding of the little things (like bringing some crackers to me and Fred during a long meeting) is something I will never forget. I have truly enjoyed my collaborations with Francois Anderegg, and am very thankful for all the times he shared his extensive understanding of experimental science. And to Nobu Shiga and Kevin Rigg, whose presence in the lab and help with the experiments was central to my success. I also thank current group members Terry Hilsabeck, Andrey Kabantsev, and Jonathan Yu, for many good discussions, both in the lab, and during the various conferences.

A special thanks goes to former group members Jason Kriesel and Eric Hollmann. Throughout the years, Jason's interest in my work and respect for my opinion managed to keep me moving forward when few things would. I am very thankful for his advice and continued friendship. Eric was the one who was hard to satisfy, his constant probing of my work always provided for interesting discussions, and generally lead me to a better understanding of my own work. His positive attitude and friendship was always welcome.

Graduate student life is difficult, but mine was made bearable by the presence of some excellent friends. Everything from Rick and the sailboat adventure and tossing some disc with Ed, to poker and boxing at Willie's; things I won't ever forget. My thanks especially to Rick Shelby, Ed Price, Willie Padilla, Syrus Nemat-Nasser, Mladen Barbic, Mara Harrall, and David Danks. And to all the others from our extended group who continue to press on. Also, a deep thanks to our own physics mom, Debra Bomar; very few of us would succeed without her constant care and encouragement.

Throughout the many years, my family has offered continued encouragement and support, even so far as to finally stop asking the question of when will I be finished. Lastly, I say thank you to my dear friend Agnieszka, who introduced me to the soothing sounds of *ERA* and *Deep Forest*; I will never forget all the deep conversations about life that we could never escape from.

This research was supported financially by the National Science Foundation (NSF grant PHY-9876999) and the Office of Naval Research (ONR grant N00014-96-1-0239).

Vita, Publications and Fields of Study

Vita

28 June 1973	Born, Bellflower, California
1995	B.S., University of California, Irvine
1993-1995	Lab Assistant, Department of Physics University of California, Irvine
1995-1998	Teaching Assistant, Department of Physics University of California, San Diego
1995-2002	Research Assistant, Department of Physics
1998	M.S., University of California, San Diego
2002	Ph.D., University of California, San Diego

Publications

1. F. Anderegg, N. Shiga, J. R. Danielson, D. H. E. Dubin, C. F. Driscoll, and R. W. Gould, "Thermally excited modes in a pure electron plasma," *Physical Review Letters*, Subm. Jan. 2002.

2. J. R. Danielson, F. Anderegg, K. M. Rigg, and C. F. Driscoll, "Landau Damping of Electron Plasma Waves in the Linear and Trapping Regimes", *Non-Neutral Plasma Physics IV*, edited by F. Anderegg, et al. (American Institute of Physics, San Diego, California, 2001).

3. F. Anderegg, N. Shiga, J. R. Danielson, and C. F. Driscoll, "Thermal Excitation of Trivelpiece-Gould Modes in Pure Electron Plasmas", *Non-Neutral Plasma Physics IV*, edited by F. Anderegg, et al. (American Institute of Physics, San Diego, California, 2001).

4. J. R. Danielson and C. F. Driscoll, "Measurement of plasma mode damping in pure electron plasmas", *Non-Neutral Plasma Physics III*, edited by J. J. Bollinger, et al. (American Institute of Physics, Princeton, New Jersey, 1999).

5. B. P. Cluggish, J. R. Danielson, C. F. Driscoll, "Resonant particle heating of an electron plasma by oscillating end sheaths", *Physical Review Letters* **81**, 353 (1998).

6. W. W. Heidbrink and J. R. Danielson, "The nonlinear saturation of beam-driven instabilities : irregular bursting in the DIII-D tokamak," *Physics of Plasmas* **1**, 4120 (1994).

7. J. R. Danielson, F. Anderegg, K. M. Rigg, and C. F. Driscoll, "Linear and Nonlinear Landau Damping of Trivelpiece-Gould Modes in Non-Neutral Plasmas," *Bulletin of the American Physical Society* **46**, 80 (2001)

8. N. Shiga, F. Anderegg, J. R. Danielson, C. F. Driscoll, D. H. E. Dubin, and R. W. Gould, "Thermal Excitation of Trivelpiece-Gould Modes in a Pure Electron Plasma," *Bulletin of the American Physical Society* **46**, 80 (2001)

9. J. R. Danielson, F. Anderegg, and C. F. Driscoll, “Damping and Trapping Oscillations of Trivelpiece-Gould Modes in Pure Electron Plasmas,” *Bulletin of the American Physical Society* **45**, 32 (2000)

10. F. Anderegg, N. Shiga, J. R. Danielson, C. F. Driscoll, and D. H. E. Dubin, “Thermal Excitation of Trivelpiece-Gould Modes in a Pure Electron Plasma,” *Bulletin of the American Physical Society* **45**, 32 (2000)

11. J. R. Danielson and C. F. Driscoll, “Plasma Mode Damping in a Pure Electron Plasma,” *Bulletin of the American Physical Society* **44**, 109 (1999)

12. B. P. Cluggish, C. F. Driscoll, J. R. Danielson, “Heating of an Electron Plasma by Oscillating Sheaths”, *Bulletin of the American Physical Society* **41**, 1605 (1996).

13. G. D. Garstka, J. Basken, J. R. Danielson, D. Dettmers, B. Foucher, L. Kress, B. Lewicki, D. Myers, M. Springer, K. Tritz, and R. J. Fonck, “First Results from the Low-Aspect-Ratio MEDUSA Tokamak”, *Bulletin of the American Physical Society* **39**, 1574 (1994).

14. J. R. Danielson and W. W. Heidbrink, “Nonlinear Dynamics of Beam-Driven Instabilities in DIII-D,” *Bulletin of the American Physical Society* **38**, 1938 (1993)

Fields of Study

Major Field: Physics

Studies in Plasma Physics
Professors Vitaly Shapiro and Valentin Shevchenko

Studies in Mechanics
Professor Ben Grinstein

Studies in Electromagnetism
Professor Tom O'Neil

Studies in Quantum Mechanics
Professor Kim Griest

Studies in Statistical Mechanics
Professors Daniel Arovas and Daniel Dubin

Studies in Galactic Dynamics
Professor Patrick Diamond

Studies in Mathematical Physics
Professor Donald Fredkin

Abstract of the Dissertation

Measurement of Landau Damping of Electron Plasma Waves in the Linear and Trapping Regimes

by

James Robert Danielson
Doctor of Philosophy in Physics
University of California, San Diego, 2002
Professor C. Fred Driscoll, Chairman

Experiments are presented on collisionless damping of standing plasma waves in pure-electron plasma columns. Specifically, the first quantitative measurements of "linear Landau damping" and "nonlinear wave-particle trapping oscillations" of $m_\theta = 0$ Trivelpiece-Gould (T-G) modes in a pure electron plasma are discussed in detail.

Linearly excited T-G standing waves are observed and the dispersion for long wavelength modes is measured. Prior experiments on T-G modes commonly showed exponential damping independent of amplitude, but no agreement with linear damping theory. In the present experiments, we characterize the damping from ultra-low amplitude thermal excitations to large amplitudes where particle trapping dominates.

At low wave amplitudes ($\delta n/n_0 < 10^{-3}$), the measured linear damping rate ($10^{-3} < \gamma_{\mathrm{L}}/\omega < 10^{-1}$) agrees quantitatively with Landau damping theory for moderate plasma temperatures ($1 < T_e < 3eV$, $3 < v_\phi/\bar{v} < 5$). This damping is

shown to be due to resonant particles; a dramatic decrease in the damping rate is observed when the resonant particles are eliminated by truncating the nominally Maxwellian velocity distribution. Surprisingly, no correspondence is found with the somewhat more subtle theory predictions of "bounce resonant damping," nor with damping due to "dephasing" in the plasma end sheaths.

At larger wave amplitudes ($10^{-3} < \delta n/n_0 < 10^{-2}$), the excited T-G wave initially damps at the Landau rate, but the wave-resonant particles become trapped in the wave potential, sloshing with frequency $\omega_T \equiv \sqrt{eE_z k_z/m}$, as first analyzed by O'Neil in 1965. This causes the wave amplitude to re-grow and oscillate in amplitude, approaching a BGK state. The measured times characterizing the first bounce oscillation are found to agree quantitatively (to about 20%) with predictions based on a self-consistent numerical calculation. Small discrepancies between the theory and the measured amplitude oscillation times are shown to be due to additional damping processes which are not dependent on the resonant particles.

At late times, a weak exponential damping of the wave is observed. Measurement of the average (nonlinear) decay rate for large amplitude waves is shown to be consistent with the collisional repopulation of the distribution function as described by Zakharov and Karpman in 1963. Measurements of the early-time wave amplitude peaks and valleys are consistent with the naively predicted plateau amplitude for a BGK state. Small discrepancies between the measured effective plateau amplitude and the expected BGK equilibrium amplitude is likely the result of extra damping from either resistive damping in the detection electronics or collisional repopulation, or both.

Chapter 1

Introduction and Summary

1.1 Introduction

This thesis is concerned with the dynamics of electrostatic compression waves propagating on a pure electron plasma column [1]. These Trivelpiece-Gould (T-G) modes are longitudinal Langmuir oscillations of the cylindrical plasma column [2]. Collisionless Landau damping of these waves occurs when electrons streaming at the wave phase velocity v_ϕ interact with the wave for many wave periods.

One of the interesting complications here is that these are standing waves, composed of two oppositely propagating traveling waves. In this case, the waves and the free-streaming electrons are reflected at the plasma boundaries after each transit of the plasma column. Since the reflections of waves and particles are quite dissimilar, it is questionable whether the waves can maintain coherence with the electrons for a long enough time for the resonant interaction to take place.

This thesis shows that, remarkably, the electrons and waves maintain coherence over many wave oscillations (at least 100 to 1000 cycles) and over many interactions with the plasma boundary. This implies that any perturbations to the wave/particle dynamics due to interactions with the boundary are actually quite weak. Thus, despite the reflection process, low amplitude waves are damped through the resonant interaction of the wave with particles traveling at the wave phase velocity as described by Landau in 1946 [3]. Further, large amplitude waves trap resonant particles causing oscillations in the wave amplitude and inhibit the damping of the wave consistent with the predictions of O'Neil [4].

In contrast to the work by Malmberg and Wharton [5], the spectrum of these standing waves is discrete rather than continuous. This precludes sevaral instabilities, such as nonlinear wave decay into sidebands [6], which can limit the lifetime of BGK states. Instead, our BGK states are limited by weak resistive wave damping due to the measurement electronics and by collisional smearing of the resonant particle distribution. BGK states have not previously been quantitatively diagnosed in this regime.

1.2 Summary

1.2.1 Background for the Experiments

Chapter 2 presents the details of the pure electron plasma apparatuses and wave measurement techniques that are used in this thesis. The geometry of the different traps is described as well as measurement of the basic plasma parameters of density and temperature.

Two basic techniques are used to study excited plasma modes: measurement of the mode spectrum and measurement of the temporal response. Since the plasma mode is similar to a simple harmonic oscillator, the two measurements are complimentary. In the spectral measurements, we sweep the excitation frequency through the mode resonance (at ω_0) and measure the response at each frequency. The damping rate γ is then obtained directly from measurement of the mode width. In the temporal measurements, we launch a short burst at the mode resonant frequency to excite the wave, and then measure the free decay of the mode. The damping rate is obtained directly from the exponential decay time of the received signal.

Measurements of the linear excitation of the wave are presented and discussed in context with the low amplitude (thermal) and high amplitude (soliton) limits. The measured transition from linear damping to the nonlinear damping regime is described. Further, the wave amplitude calibration is checked by directly measuring the density difference between the two ends for a large amplitude T-G wave.

The finite resistance of the wave detection circuit causes weak damping of the excited plasma mode. Measurement of the resistive damping rate γ_{load} from an imposed "RLC" circuit are shown to agree well with theoretical predictions, verifying that resistive dissipation of the mode sets a lower limit on the measured mode damping rates. For the present experiments, the limit is $\gamma_{load}/\omega_0 \gtrsim 10^{-4}$.

1.2.2 Trivelpiece-Gould Modes and Linear Landau Damping

In Chapter 3, the physics of Trivelpiece-Gould (T-G) modes and the measurements of linear Landau damping are presented and compared to theory.

The waves studied in this thesis are long wavelength, azimuthally symmetric ($m_\theta = 0$) T-G modes. An overview of the derivation of mode dispersion is presented as well as measurements of the first 10 standing wave frequencies verifying the numerically calculated T-G dispersion relationship. Except for this verification of the dispersion equation, all experiments will consider only the dynamics of the lowest frequency, longest wavelength ($m_z = 1$) mode. This mode is commonly referred to as the "sloshing" mode because the center of mass shifts from end to end. The density and potential variation is peaked near the ends of the column with a half-wavelength approximately equal to the plasma length.

The theory of linear Landau damping is presented as well as the numerical code used to calculate the theoretical damping rate. Linear damping rate measurements are made with 3 techniques: driven spectral response, thermal spectrum measurement, and temporal decay of a pulse excited wave. These techniques give identical measured damping rates in the range of $10^{-3} < \gamma_{\mathrm{L}}/\omega < 10^{-1}$ and are in quantitative agreement with linear Landau damping theory for plasma temperatures giving $3 \lesssim v_\phi/\bar{v} \lesssim 5$.

An experiment is presented where the velocity distribution is truncated at high velocities by a slight “hollowing” of the plasma column. A factor of 10 decrease in the damping rate is observed when the hollowing level is sufficient to remove most electrons with velocities at (and above) the wave phase velocity. This demonstrates the necessity of resonant particles in order to damp the wave at the Landau rate.

The theory of bounce resonant damping is introduced and a simple model is used to calculate the theoretical damping rate. Bounce resonant damping is an enhancement over Landau from the coupling of the standing wave to harmonic resonances of the plasma column. No agreement is found with the experiments and the predictions from the simple model.

Further, no agreement is seen between the measured damping rates and calculations of wave damping from the dephasing of the electron velocity perturbation at the end sheaths.

1.2.3 Non-linear Trapping Oscillations

In Chapter 4, the measurements are extended from the low amplitude linear regime to the large amplitude regime where the trapping of resonant particles in the wave potential becomes important. A launched wave initially damps linearly, reaches a minimum ("valley") amplitude, then re-grows to a peak amplitude somewhat less than the launched amplitude.

The theory of O'Neil predicts these amplitude oscillations, and a simple numerical treatment is presented which avoids some of the approximations used in the theory. The time it takes for the first amplitude oscillation gives the trapped particle "bounce frequency" ω_B and is shown to be in good agreement (to about 20%) with the numerical calculations. Further, the measured time to reach the first amplitude valley τ_{vall} is also found to be in excellent agreement (to about 5%) with the predictions from the numerical calculation.

Measurements of the amplitudes of the bounce oscillation and valley depth are also presented. Although the valley depth is in excellent agreement with the numerical calculations, the peak bounce amplitude obtained at the lowest launched amplitudes differs from the theory by as much as a factor of 3. This is shown to be most likely caused by resistive damping or collisional effects, neither of which is accounted for in the basic theory.

The long-time (nonlinear) decay rate of the mode is measured, and found to be consistent with the rate expected due to collisional repopulation of resonant particles.

Lastly, the numerical calculations predict that in the long time limit, the trapping oscillations phase-mix to a steady-state amplitude (plateau), sometimes referred to as a "BGK equilibrium." Measurements of the long-time plateau level are shown to be somewhat lower than expected from the theory, by as much as a factor of 2 for the lowest amplitude waves.

Chapter 2

Background for the Experiments

2.1 Overview

This chapter describes the non-neutral plasma traps and the experimental techniques used to measure the damping of plasma waves. There were 3 different traps used for the experiments, all cylindrical devices, typically referred to as Penning-Malmberg traps. The waves are launched and detected by applying voltages to and detecting voltages on isolated cylindrical electrodes. For all the experiments in this thesis, the waves are cylindrically symmetric ($m_\theta = 0$).

Two techniques are used to measure the damping of plasma modes. First, the frequency spectrum of the mode was measured by either externally sweeping through the mode resonance, or by the detection of the thermally excited mode spectrum. Second, the time evolution of decaying modes was measured by pulse excitation of the mode with a fixed number of cycles. The spectral measurements give the same information as the temporal response of the mode but allow for increased sensitivity by utilizing longer time averages. The pulse-decay excitation typically has a worse signal-to-noise, but allows for detailed investigation into the temporal response of the modes.

Lastly, the effect of the finite impedance of the detection circuit will be

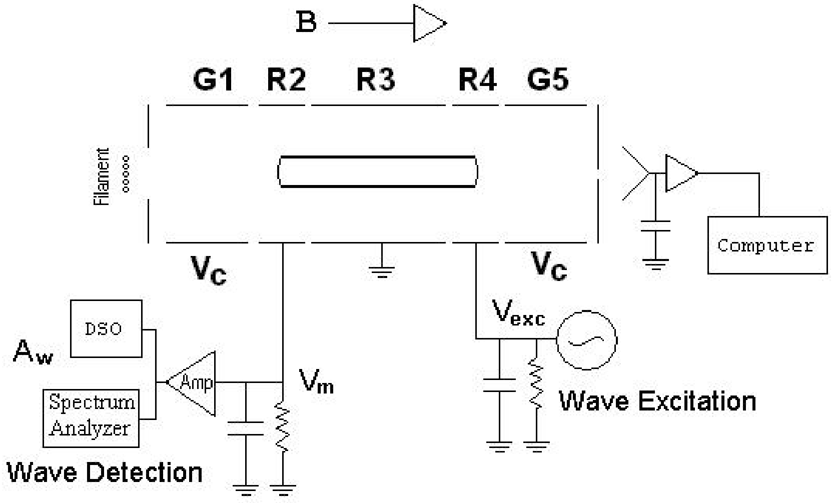

Figure 2.1: Penning-Malmberg trap schematic showing the location of the excitation and detection electrodes for the wave experiments. The experiments typically set $V_C = -100V$.

detailed. Experiments which demonstrate the damping of plasma modes due to an external circuit impedance will be presented and shown to compare well with the theoretical predictions.

2.2 Pure Electron Plasma Traps

Three different Penning-Malmberg electron traps were used (EV, IV, CV), all represented schematically by Figure 2.1. The traps consist of series of isolated hollow cylindrical electrodes in ultra-high vacuum with pressure $P < 10^{-10}$ Torr. The electrons are confined radially by a uniform magnetic field ($0.4 < B < 40$kG) and axially by confinement voltages $V_c \approx -100$ Volts. Waves are excited with a signal generator with voltage V_{exc}, V_m is the detected voltage on the receiving electrode, G is the linear gain of the amplifier, and A_w is the amplified (and filtered) voltage measured on either the oscilloscope or spectrum analyzer.

The principle differences between the three traps are magnetic field strength

Parameter	EV	IV	CV
Magnetic field, B_z	380G	30kG	40kG
Wall Radius, R_w	3.81cm	2.86cm	1.27cm
Plasma Radius, R_p	1.5cm	0.2cm	0.05cm
Plasma Length, L_p	30cm	41cm	8cm
Total Charge, Q_{tot}	10^9	10^9	10^8
Central Plasma Density, n_0	10^7cm^{-3}	$2 * 10^8\text{cm}^{-3}$	10^9cm^{-3}
Plasma Temperature, T_e	$0.5 - 3$eV	$0.1 - 2$eV	$0.05 - 2$eV
Plasma Frequency, $\omega_P/2\pi$	28MHz	127MHz	280MHz
$m_z = 1$ Mode Frequency, f_0	3.0MHz	2.0MHz	10.0MHz
For $T_e = 1$eV	$v_\phi/\bar{v} \approx 5.6$	$v_\phi/\bar{v} \approx 3.9$	$v_\phi/\bar{v} \approx 4.8$
$\nu_{ee} = \frac{16}{15} n\bar{v}b^2 \ln(\frac{r_c}{b})$	$\approx 180\text{sec}^{-1}$	$\approx 2000\text{sec}^{-1}$	$\approx 9000\text{sec}^{-1}$

Table 2.1: Typical parameters for 3 different pure electron plasma traps.

and typical plasma radius. Table 2.1 lists the main experimental parameters for the different traps labeled EV, IV, and CV, respectively.

The traps are operated in the standard inject-hold-dump cycle, typical of Penning-Malmberg traps [7, 8]. Referring to Figure 2.1, the voltage on gate $G1$ is lowered to ground to allow electrons from the filament to stream into the confinement region. After a short fill time, $G1$ is returned to the confinement voltage V_C. There is a short delay time after injection to allow the electrons to come to an equilibrium, then the wave excitation and detection is performed. Gate $G5$ is then lowered to ground to allow the electrons to stream out of the confinement region. After the electrons are removed, $G5$ is returned to voltage V_C and the cycle is repeated.

The z-integrated density is measured by dumping the plasma through a movable hole onto a Faraday cup. A typical density profile from the EV machine is shown in Figure 2.2. Here the measured density is plotted as a function of the radial position of the hole in the collector plate. Each point is the average of 4 identical experimental cycles. The shot-to-shot variation in the total charge is typically less

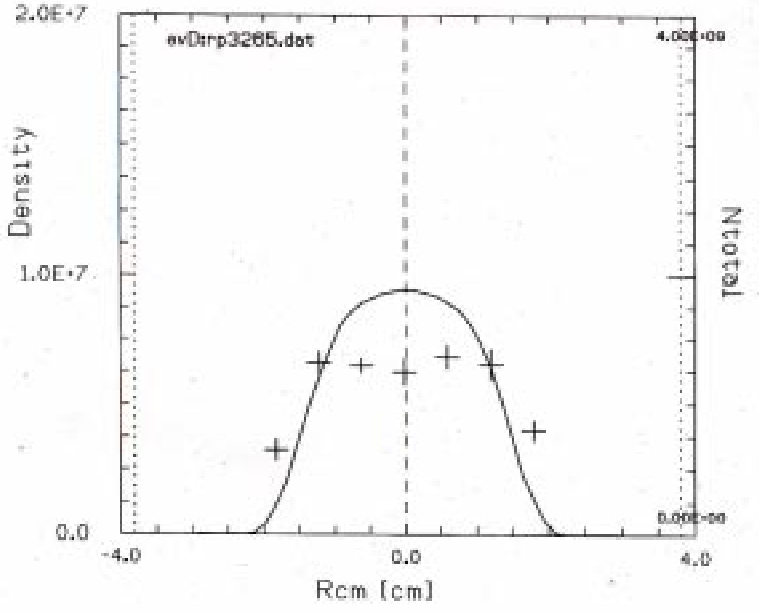

Figure 2.2: Typical measured EV density profile.

than 0.1%. The electron source for CV and IV is in the fringing magnetic field, so the electrons are compressed to a smaller radius and correspondingly a higher density upon injection into the trap.

The EV machine incorporates a magnetic "beach analyzer" for measurement of the perpendicular plasma temperature [9]. This analyzer is used to measure the radial profile of the plasma temperature (shown as the crosses in Figure 2.2).

The parallel temperature is measured on all machines by slowly ramping the dump gate voltage while measuring the collected charge as a function of confinement voltage. The escaping charge is fit to the exponential tail of a Maxwellian, giving a temperature estimate that is accurate to about 10% for temperatures $T \gtrsim 0.1$ eV [10]. This technique gives only the parallel temperature on axis ($r = 0$) [10].

The relatively rapid perpendicular-to-parallel thermal equilibration rate $\nu_{\perp\parallel} = \frac{8\sqrt{\pi}}{25} n b^2 \bar{v} \ln(\frac{r_c}{b}) > 10^2 \text{ sec}^{-1}$ [11, 9] allows these experiments to be described by a single temperature $T_\perp = T_\| \equiv T$. Here $b = e^2/T$ is the classical distance of closest approach, r_c is the cyclotron radius, n is average plasma density, and $\bar{v} = \sqrt{T/m}$ is the electron thermal velocity. Furthermore, any radial temperature variations are small enough to be ignored here.

A separate signal generator is usually attached to cylinder R3 to provide controlled heating of the plasma [12]. The heating frequency is set close to the thermal bounce frequency $\bar{f}_b = \bar{v}/2L_P$, which is less than 1/3 of the mode resonance frequency $(\omega/2\pi)$, assuring no coupling to the plasma mode to be studied. Further, a switch can be used to physically disconnect the heating circuit after heating in order to minimize the effect of the circuit on the subsequent wave dynamics.

2.3 Wave Measurements

2.3.1 Spectral Measurements

The frequency spectrum of the modes is measured by utilizing a spectrum analyzer and a tracking generator. In order to get an accurate measure of the mode width (and hence the damping rate), the spectrum analyzer bandwidth BW must be smaller than the mode width. This limits the ability to detect the smallest damping rates: the smallest width that can be measured is the bandwidth of the spectrum analyzer. The strongly damped waves are broad, and thus their measurement is limited by the signal-to-noise of the amplifier.

An example mode width measurement is presented in Figure 2.3. Here the generator frequency is swept from below the mode resonance to above the resonance with a constant amplitude excitation. The peak response (V_{pk}) and the mode full-width at half-maximum (Δf) are directly measured from the data. The damping rate is then found from $\gamma/2\pi \equiv \Delta f/2$.

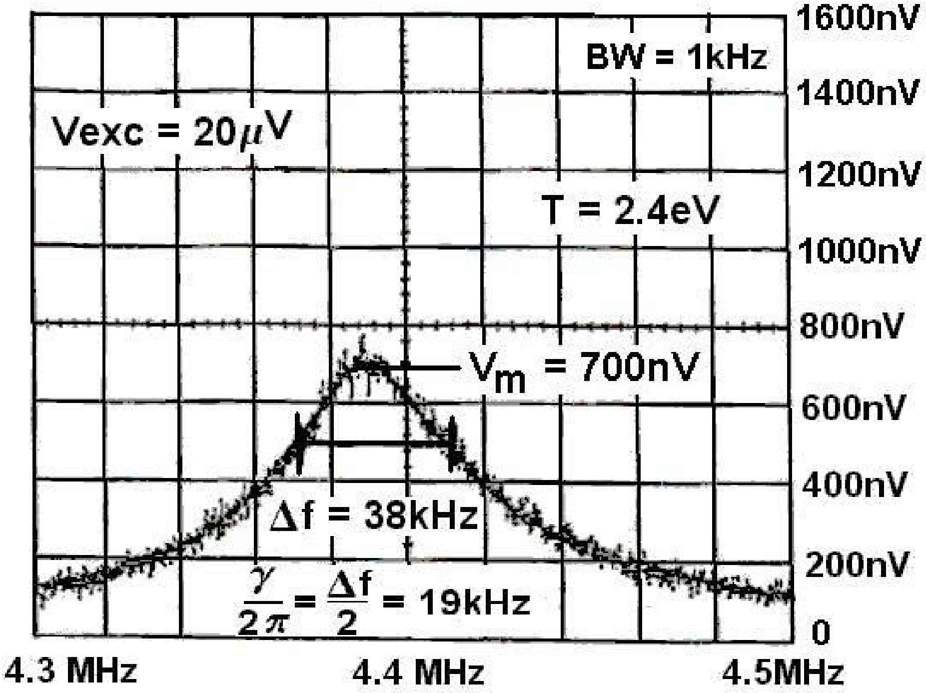

Figure 2.3: Measured plasma response as a function of applied frequency. The width of the resonance is proportional to the mode damping rate.

2.3.2 Temporal Measurements

For the pulse-decay measurements, the T-G modes are excited by a short burst (for 10 cycles, ie. $N_{cyc} = 10$) at the wave resonant frequency ($\omega_0/2\pi$) applied to cylinder R4 as shown in Figure 2.1. The resulting wave density fluctuations induce image charges on cylinder R2; the image charges are detected using either a charge amplifier (input impedance $\sim 4\Omega$) or a low-noise 50-ohm RF amplifier. The received signal is filtered and fed into a RF spectrum analyzer tuned to the resonant frequency with a bandwidth of 300kHz.

The analyzer bandwidth also limits the temporal measurements. In this case, too small of a bandwidth limits the response time of the analyzer, thus making it difficult to measure modes with large damping rates. The weakly damped modes,

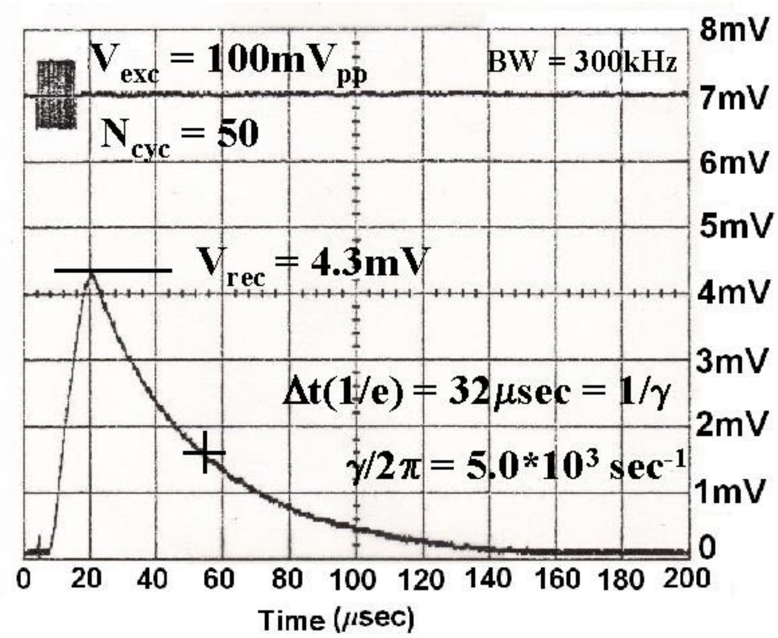

Figure 2.4: Measured wave potential at the wall as a function of time after a pulse excitation at the mode resonant frequency.

on the other hand, are detected with great efficiency.

For these experiments we launch the $m_\theta = 0, m_z = 1, m_r = 1$ Trivelpiece-Gould standing wave, also known as the "sloshing" mode. This is the longest wavelength longitudinal oscillation of the plasma column; it has nodes of the axial electric field E_z at the ends, and a wavelength $\lambda \approx 2L_P$ (see Section 3.2).

An example of the temporal measurement is presented in Figure 2.4. Here a function generator emits a pulse of 10 cycles at the resonant frequency to excite the wave. The wave potential at the wall is amplified and detected on the spectrum analyzer with a bandwidth BW = 300kHz. The exponential decay of the mode is measured to obtain γ; ie. $A_w = V_{pk}\ \exp[-\gamma t]$. The magnitude of the signal on the electrode (V_m) is found by dividing the peak signal by the amplifier gain, ie. $V_m = V_{pk}/G$.

2.3.3 Linear Excitation and Nonlinear Damping

We consider three levels of excitation of waves in plasmas. At the lowest amplitude, there exist thermally-excited oscillations. The weakly damped modes are excited at a non-zero amplitude due to the thermal fluctuations of the plasma particles [15]. At higher levels of excitation, we have linear coupling to a damped harmonic oscillator. In this linear excitation regims, the wave amplitude is basically linearly proportional to the voltage applied to the wall. At even higher amplitudes, the plasma will eventually reach a level of saturation and excite solitons, or other non-linear waves [16, 17, 18].

This thesis is concerned only with linear waves, meaning that the amplitude of the wave is linearly proportional to the excitation level, while the damping rate may or may not depend on the amplitude of excitation. Thus, unless otherwise noted, we exclude the largest amplitude levels, and only take data in regions where the wave is linearly excited.

Figure 2.5 shows the damping rate $\gamma/2\pi$ from measured spectral width (hollow circles) versus excitation amplitude; along with the corresponding received peak voltage V_m (solid squares) versus excitation amplitude, for a hot plasma with $T \approx 2.4$eV.

For very low applied excitation V_{exc}, the received mode amplitude V_m is independent of V_{exc}, and is due to thermal excitation of the mode (see Section 3.4.1). In this low amplitude regime, the measured damping rate $\gamma/2\pi$ is seen to be independent of mode amplitude, representing linear Landau damping or other linear damping as discussed in Section 3.4.

For larger amplitudes ($V_{exc} > 10\mu$V), the damping rate decreases with increasing amplitude by as much as a factor of 10, signifying the nonlinear damping regime. This transition to nonlinear damping is shown in Chapter 4 to be due to

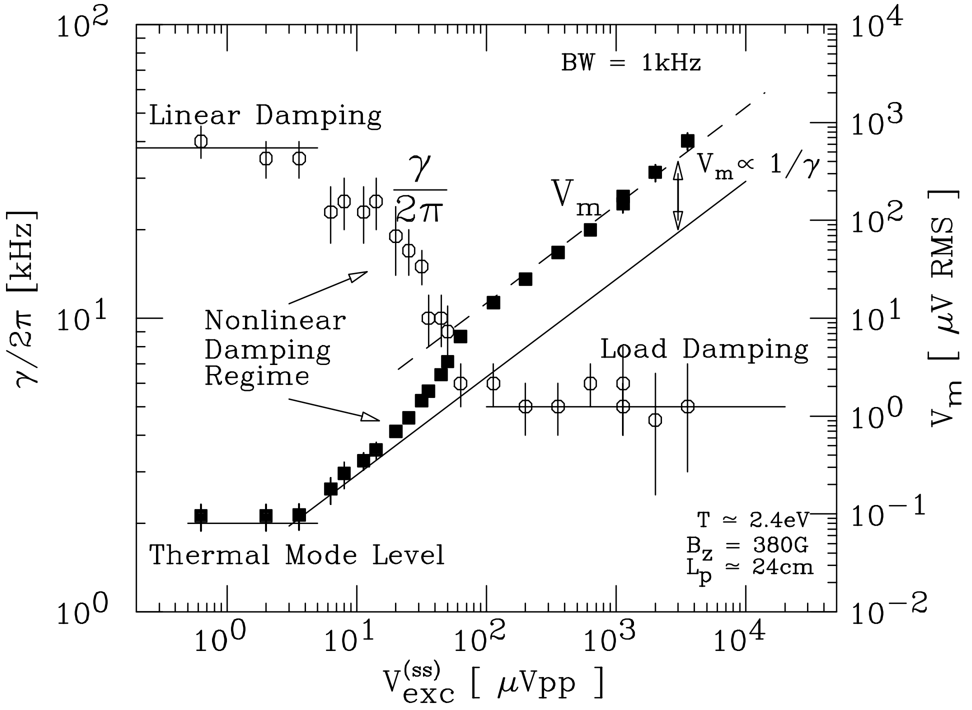

Figure 2.5: Linear and nonlinear T-G spectrum measurement on EV.

the trapping of resonant electrons in large amplitude waves. In this nonlinear regime, the measured peak response is observed to rise faster than linear with the excitation amplitude.

This apparent nonlinearity is because the damping affects the excitation level of the wave; it is not due to the excitation of a nonlinear wave. This is understood by remembering that for a driven simple harmonic oscillator at a fixed excitation amplitude, as the damping is decreased, the steady-state peak response on resonance will be increased. This implies that $V_m \propto 1/\gamma$ which is qualitatively consistent with the measurements in Figure 2.5.

The spectral width measurement, essentially, measures the steady-state response of the system at each frequency. This is equivalent to burst excitation at a single frequency for a long enough time such that a steady-state amplitude is

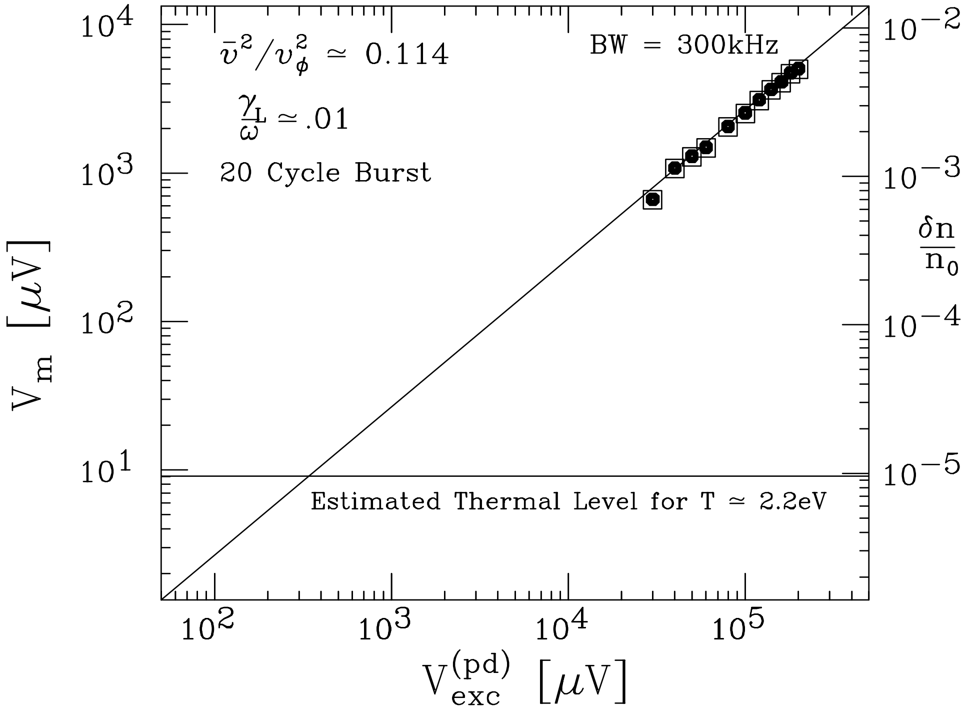

Figure 2.6: Received amplitude vs. excitation amplitude. The solid line is the linear coupling curve. Also shown is the expected thermal mode level on the same scale.

reached; ie. much longer than a damping time. This is written as $N_{cyc} \gg \omega/\gamma$, where ω/γ is approximately the number of cycles in a damping time. This is in contrast to the pulse-decay excitation where a short burst with $N_{cyc} \lesssim \omega/\gamma$ is used to excite the wave. For this case, the wave does not reach a steady-state amplitude, but rather $V_{pk} \propto V_{exc}N_{cyc} < V_{ss}$, where V_{ss} is the equivalent steady-state amplitude that would be reached for large enough N_{cyc}. This means that for a short-time scale excitation, nonlinear damping of the wave will not affect the excitation amplitude of the wave.

Figure 2.6 shows the received amplitude versus excitation amplitude for a temporal decay experiment, where the wave is excited by a short burst with $N_{cyc} = 20 < \omega/\gamma = 100$. Here the peak amplitude at the wall V_m is plotted as a function of the excitation voltage V_{exc}. The data shows a linear response between the excited voltage and the detected peak wave amplitude. In contrast to the spectral mode width measurement in Figure 2.5, no nonlinearity of the received peak response is observed. Although this is for a different plasma, the solid line is Figure 2.6 represents the same coupling as the solid line in Fgwidth.nonlin.

For reference, the calculated density perturbation level is given on the right hand axis. Also shown is the expected level for thermally excited plasma waves which are further discussed in Chapter 3.

2.4 Amplitude Calibration

An absolute calibration of the mode amplitude is obtained from measurement of the density variation in the mode by dumping half of the plasma column. This technique is a slight modification of the well developed technique of phase-locked density measurements of the diocotron mode (eg. Reference [13], or more recently [14]). Since T-G modes are longitudinal in nature, dumping the entire plasma would “smear out” the perturbation by averaging over all z during the dump. In this case, we phase lock to a large amplitude wave excited by the pulse-decay method and dump only half the plasma synchronous with the wave. For these measurements we use a cold plasma which shows no fast damping so as to maximize the number of cycles we can average over without introducing errors.

A circuit was developed to quickly “cut” the plasma in half. This cutting is done by placing a large voltage ($V_{cut} \gg \Phi_{Sp}$, where Φ_{sp} is the plasma space charge) on the middle electrode in a time less than the mode period. Since the density perturbation is odd in z, this will contain half of the perturbation on one side of the cut, and half on the other side. Then the side closest to the dump gate is dumped and measured. The time of the “cut and dump” is changed in phase

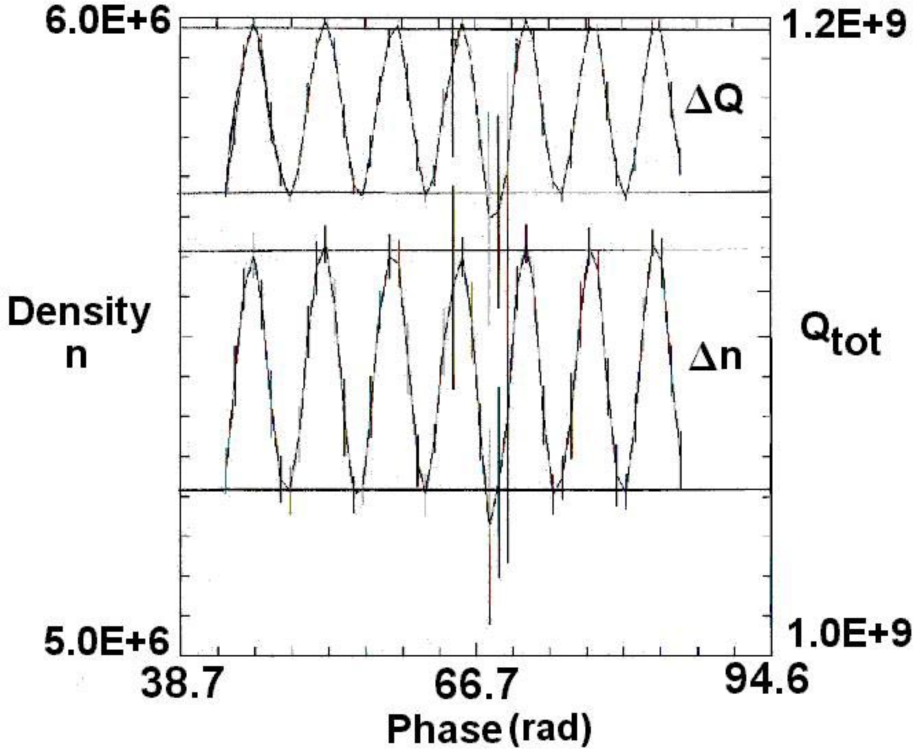

Figure 2.7: Collected density Δn on axis and "total" charge ΔQ from one half of the column, as a function of wave phase.

with the excited wave; thus obtaining a measure of dumped density as a function of wave phase.

An example of the phase-locked "cut and dump" measurement is shown in Figure 2.7, where the measured density through the collector hole and the measured total charge in half the plasma are plotted versus time delay (phase $= (\omega_0/2\pi)\Delta t$) between mode excitation and the "cut." We measure the half-column density over several wave cycles (typically 5 or more) and average to find the magnitude of the variation Δn. This technique is expected to be good to about 10%, mostly limited by the shot-to-shot noise and the fact that the cut gate is not exactly in the middle of the plasma.

As shown in the Appendix, from the mode dispersion equation we calculate the relationship between the density perturbation δn and the measured detector voltage V_m. From Equation A.7 and Equation A.10, we find

$$\frac{\delta n}{n_0} = \frac{2}{\hat{f}} \frac{\ln(R_w/R_p)}{J_0(x)} \frac{e}{m v_\phi^3} \frac{V_m}{R_f} \tag{2.1}$$

where $\hat{f}$ is a coupling constant obtained from the geometry of the detection electrode, and $x \equiv k_z R_p \sqrt{(\omega_p/\omega)^2 - 1}$.

From the measurement of the wall voltage and the measured δn we calculate the geometric coupling between the density perturbation and the radial electric field on the detection electrode (at $r = R_w$). We find agreement to about 20% with Equation 2.1.

2.5 Resistive Damping

If the plasma has some internal damping mechanism (ie. linear Landau damping), the inherent plasma impedance Z_p due to the damping is proportional to the damping rate γ_p/ω_0. This proportionality was shown in Section 2.3.3; as the damping rate decreases, the measured peak received amplitude increased, just as would be expected if the Load impedance (in this case the plasma impedance) decreased. The physical mechanism of this internal damping is the subject of Chapter 3, and the nonlinear decrease at large amplitudes the subject of Chapter 4.

However, in an identical way, an external impedance will also cause a finite level of dissipation of the plasma wave, with a damping rate γ_{load}/ω_0 proportional to the real part of the applied load impedance $Re\{Z_{load}\}$. The calculation of the damping rate from resistive dissipation in the external impedance follows from Reference [15]. The mode equation is solved with a finite arbitrary impedance on the detection electrode, whose real part is given by $Re\{Z_{load}\}$. This is similar to the calculation of the resistive wall instability of slow-waves on space charge dominated electron beams [19, 20, 21].

The total damping rate of the wave γ_{tot}, including both internal plasma damping γ_p, and external load damping γ_{load}, is found to be

$$\frac{\gamma_{\rm tot}}{\omega_0} \equiv \frac{\gamma_p}{\omega_0} + \frac{\gamma_{load}}{\omega_0} = (Re\{Z_p\} + Re\{Z_{load}\})\ \omega_0\ \mathcal{G}, \tag{2.2}$$

where the geometry factor $\mathcal{G}$ is given by

$$\mathcal{G} \equiv L_p\ \frac{\mathcal{J}(x)}{\pi^2}\left[\sin\left(\frac{\pi(z_c + L_c)}{L_p}\right) - \sin\left(\frac{\pi z_c}{L_p}\right)\right]^2$$

with

$$\mathcal{J}(x) \equiv [J_0^2(x) + J_1^2(x)]/(\partial D/\partial x)^2$$

and $D(x) \equiv xJ_1(x)\ln(R_w/R_p) - J_0(x)$ and $x \equiv (\omega_p^2/\omega_0^2 - 1)^{1/2}k_zR_p$. ω_0 is used to refer to the resonant frequency of the mode, since in general, Z_{load} will depend on the excitation frequency. For EV, putting in the experimental parameters and electrode location, the theory predicts $\gamma_{load}/\omega \approx Re\{Z_{load}\}/130\text{k}\Omega$ for the test circuit described below.

Damping rate measurements are made using a test circuit composed of an inductor L, a capacitor C, and a variable resistor R_{var}, as shown in Figure 2.8. This circuit is attached to a separate electrode from the excitation and detection circuits, so the measured damping rate will consist of components from all attached circuits. From elementary circuit theory, the Real part of the impedance is found to be

$$Re\{Z_{load}\} = Re\{Z_{RLC}\} = R_{var}\frac{\omega^2L^2}{\omega^2L^2 + R_{var}^2(1-\omega^2LC)^2} \tag{2.3}$$

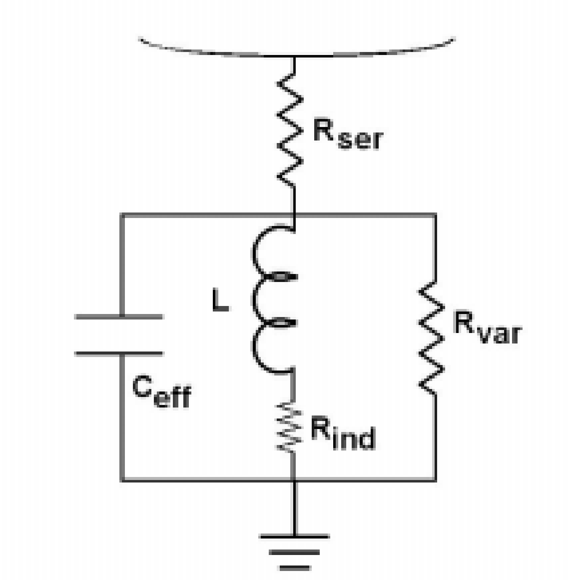

Figure 2.8: Circuit for measuring resistive damping.

where R_{var}, L, and C, are the circuit resistance, inductance and capacitance, respectively. An extension to Equation 2.3 including the effective resistance of the inductor R_{ind} and an extra series resistor R_{ser}, to account for the extra impedance from the excitation and detection electrodes, is used to fit to the measurements.

An impedence meter is used to measure the magnitude and phase of the circuit impedence at the mode frequency ($f_0 \sim 3.0$MHz) for each resistor value used. Note that the effect of the inductor is to partially cancel the effect of the capacitance in the circuit, in order to maximize the range of $Re\{Z\}$.

Figure 2.9 shows the measured real part of the circuit impedance as a function of resistor value. The dashed curve shows the expected values calculated using Equation 2.3 and the independently measured values for C, L, and R_{ind} (the small finite resistance of the inductor is the main factor in the limit as $R_{\mathrm{var}} \to \infty$). The solid curve is a best fit with the free parameters of R_{var} (for large R) and R_{ser} (for small R), which accounts for the presence of other damping mechanisms. The best fit values are well within the uncertainty of the measured values.

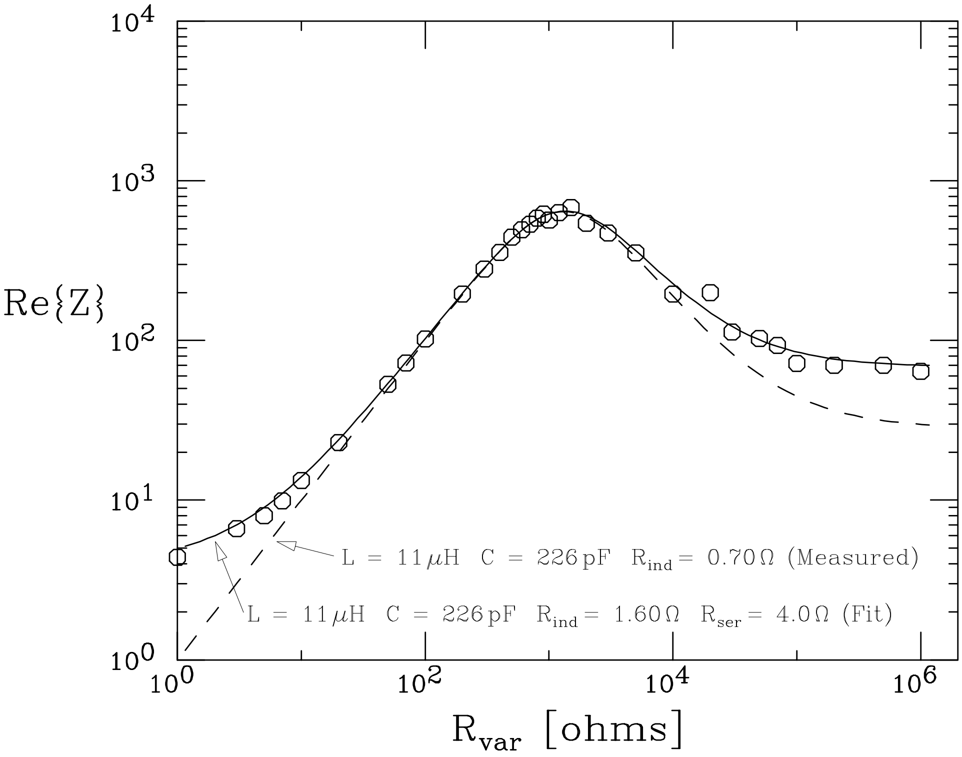

Figure 2.9: Measured Re{Z} vs. measured circuit resistance (R_{var}). The dashed curve is the theoretical prediction based on the measured values of the circuit components. The solid curve is a best fit, including an extra series resistor which accounts for stray impedances not included in the simple circuit picture.

The plasma mode damping rate caused by this circuit is found to be linearly proportional to the measured Real part of the circuit impedance. Figure 2.10 shows the measured total damping rate γ_{tot}/ω versus $Re\{Z\}$ for a large amplitude wave on a cold plasma with negligible internal (Landau) damping $\gamma_p/\omega < 10^{-4}$. The data is seen to roughly lie on a straight line with a small vertical offset, as predicted by Equation 2.2.

This resistive damping sets a lower limit to the measurements of γ/ω that can be made in these traps. For instance, extensive use of the charge amplifier (described above), minimizes the effect of the detector impedance and was used for the nonlinear trapping measurements in Chapter 4. However, it is practically

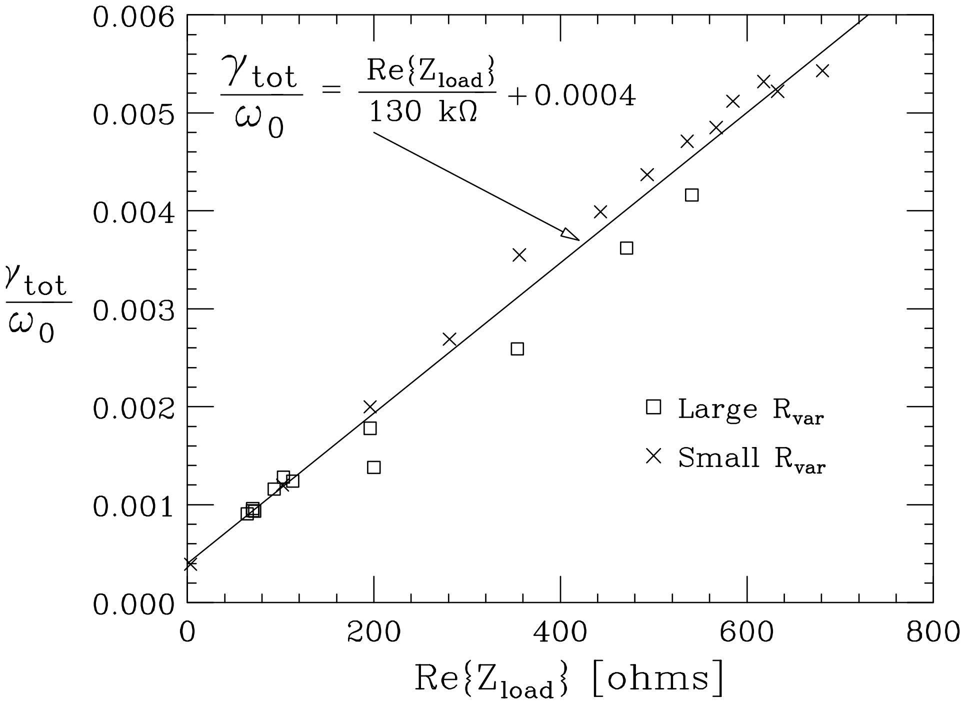

Figure 2.10: Measured damping rate (γ/ω) vs. measured Re{Z} for the data presented in Figure 2.9. The solid curve is the theoretical prediction based on the geometry and plasma parameters as explained in the text. The non-zero damping rate for Re{Z} → 0 is due to some other inherent damping that is not resistive (eg. Landau, etc.).

impossible to get less than 1 Ohm impedance, which would correspond to a limit of $\gamma/\omega \sim 10^{-5}$. This appears to be achievable with judicious choice of detector impedance (currently, we are limited to $\gamma/\omega \sim 5 * 10^{-5}$).

Chapter 3

Trivelpiece-Gould Modes and Linear Landau Damping

3.1 Overview

This chapter presents the first measurements of Landau damping in the linear regime in trapped pure electron plasmas. Section 3.2 describes the physics of Trivelpiece-Gould (T-G) modes, including measurement of the wave dispersion. Section 3.3 presents the basics of the linear theory and highlights the relevant formulas. The numerical code used to calculate the theoretical damping rates is discussed, as well as limits to the linear theory. Measurements of the linear damping rate are presented in Section 3.4, and shown to agree closely to the absolute predictions of the theory for both spectral and temporal experiments. Further, experimental modification of the electron velocity distribution function verifies the necessity of the resonant particles in the damping. Lastly, the linear damping rate measurements are compared to the predictions of bounce resonant harmonic damping and sheath damping in Section 3.5.

3.2 Trivelpiece-Gould Modes

We consider electrostatic compression waves (Langmuir waves) propagating axially on the pure electron column, in the linear regime where $\delta n/n \ll 1$. Trivelpiece-Gould (T-G) modes are these electron plasma waves in the regime where a bounding cylindrical wall limits the maximum phase velocity of waves for long wavelength modes.

Put simply, the grounded conducting walls force the wave electric field to be perpendicular (ie. $E_r \neq 0, E_z = 0$) at the wall (shown pictorially in Figure 3.1). This limits the maximum axial electric field on axis when the wavelength is comparable or larger than the tube radius $(R$). So, unlike Langmuir oscillations which

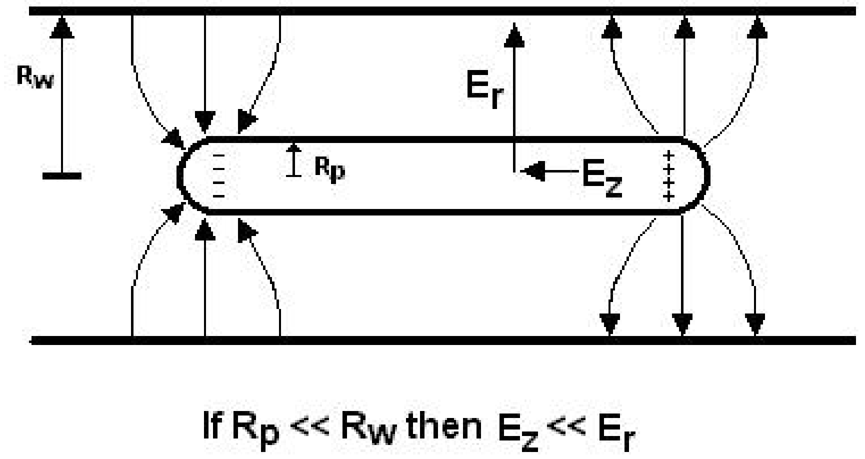

Figure 3.1: A simple picture of the lowest order T-G mode on a plasma column.

becomes

$$\omega^2 = \omega_p^2 \frac{k_z^2}{k_{tot}^2} + 3\bar{v}^2 k_z^2 \tag{3.1}$$

where $\omega_p \equiv \sqrt{4\pi n e^2/m}$, $k_{tot}^2 \equiv k_z^2 + k_\perp^2 \approx k_\perp^2$, and $k_\perp \approx \frac{1}{R_p}\left[\frac{2}{\ln{(R_w/R_p)}}\right]^{1/2} \gg k_z \approx \pi/L_p$, for the experiments in this thesis. It is apparent from Equation 3.1 that as k_z becomes larger than $k_\perp$, the reduction factor approaches unity, and the plasma waves are the same as in an infinite plasma [23].

Figure 3.2 pictorially presents the T-G dispersion relation where ω/ω_p is plotted versus $k_z/k_\perp$ [24]. The plot also labels different regions of the dispersion curve in

ri-

ments.

1,

$m_r = 1$

ss”

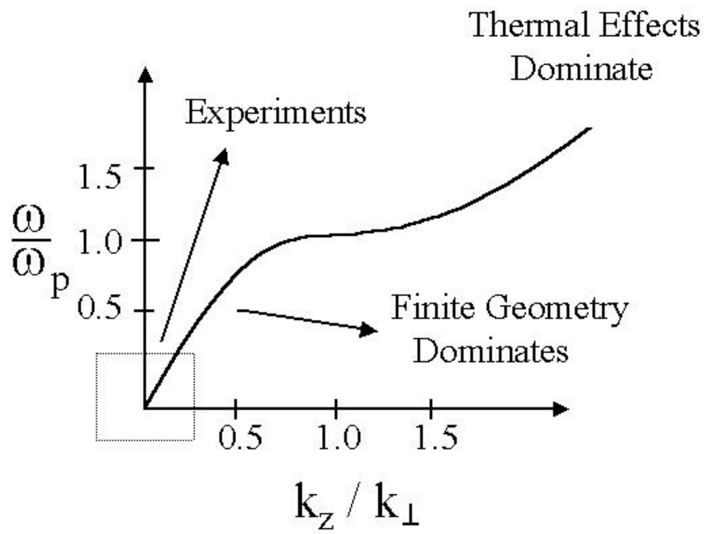

Figure 3.2: A picture of the $m_\theta = 0$ T-G mode dispersion showing the location of the experiments.

mode. This is the longest wavelength longitudinal oscillation of the plasma column. It has nodes of E_z (and anti-nodes of potential and perturbed density) at the ends (Figure 3.1). This means that the wavelength λ is approximately twice L_p, with wavenumber $k_z = 2\pi/\lambda \approx \pi/L_p$.

Jennings et al. demonstrated with numerical simulations that the finite length of the plasma column acts to slightly increase the effective wavelength [25], thus making the effective wavenumber k_z^{eff} slightly smaller than π/L_P. Numerical solutions of the drift-kinetic equations for an infinite-length column with a given density profile $n(r)$ and plasma temperature T, determine a wavenumber k_z^{∞} which gives the observed mode frequency ω [26]. We presume that the finite-length column has $k_z^{\mathrm{eff}} = k_z^{\infty}$ obtained from the numerical calculation, and calculate the wave phase velocity as $v_\phi = \omega/k_z^{\mathrm{eff}}$. Thus, the expected plasma dispersion equation becomes

$$f_{mode} = \frac{\omega}{2\pi} \approx \frac{\omega_p}{2\pi}\, k_z^{eff} R_p \, \left[\frac{1}{2}\ln\left(R_w/R_p\right)\right]^{1/2} \, \left[1 + \frac{3}{2}\left(\frac{\bar{v}}{v_\phi}\right)^2\right] . \tag{3.2}$$

Equation 3.2 is plotted as the solid line in Figure 3.3.

We measure the frequency of the normal modes by sweeping the excitation frequency through the resonance frequency as described in Section 2.3. The data from one such experiment is presented in Figure 3.3 along with predictions from the “DriftK” numerical code. The excellent agreement of the measured frequency with the predictions from the code verifies our identification of the modes and gives us confidence in our estimates of the wave phase velocity as described above.

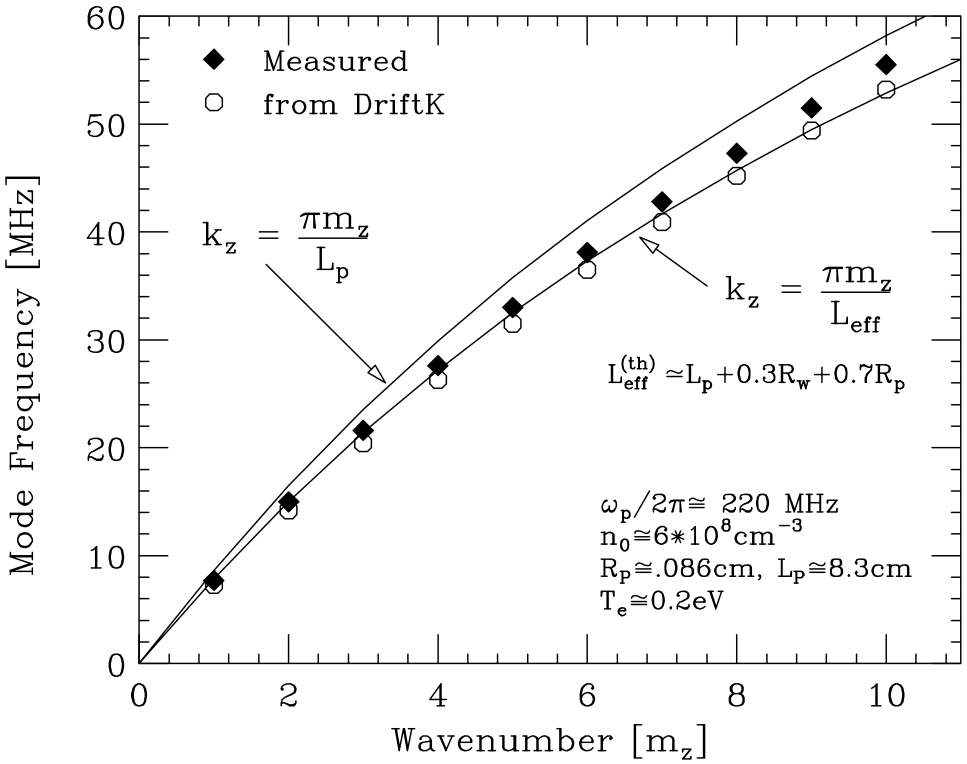

Figure 3.3: Measured dispersion on CV. The dashed line is from "DriftK" numerical calculations using the measured plasma density profile and temperature.

3.3 Landau Damping

3.3.1 Linear Theory

Landau damping results from the resonant interaction of electrostatic waves with particles traveling at the wave phase velocity, $v_\phi = \omega/k_z$. Depending on the slope of the particle velocity distribution at v_ϕ, this resonant interaction can cause either wave damping or wave growth [3, 27]. For Langmuir waves in an infinite homogeneous plasma, Landau calculated a temporal damping rate γ_{LD} given by

$$-\frac{\gamma_{LD}}{\omega} \equiv \frac{Im[\omega]}{\omega} \cong \frac{\pi}{2}\, v_\phi^2\, \frac{\partial f_0}{\partial v}\Big|_{v_\phi} \qquad (3.3)$$

When the distribution function is Maxwellian, $f_0 = \frac{1}{\sqrt{2\pi}}\frac{1}{\bar{v}}\ \exp\left[-\frac{1}{2}\left(\frac{v}{\bar{v}}\right)^2\right]$, where $\bar{v} \equiv \sqrt{T/m}$, Equation 3.3 becomes

$$\frac{\gamma_{LD}}{\omega} \approx \sqrt{\frac{\pi}{8}} \left(\frac{v_\phi}{\bar{v}}\right)^3 \exp\left[-\frac{1}{2}\left(\frac{v_\phi}{\bar{v}}\right)^2\right]. \tag{3.4}$$

This equation comes from an expansion of the plasma dispersion function[28] to lowest order in the parameter $\bar{v}/v_\phi$ [29]. In the spatial damping experiments by Malmberg [5], a similar expression for k_i/k_r (k_i is the damping length, $k_r = 2\pi/\lambda$) was tested by varying the wave phase velocity (by changing the wave frequency) and measuring the corresponding spatial damping length k_i using a plasma at a fixed temperature.

From Equation 3.2, we find the wave phase velocity as

$$v_\phi \equiv \frac{\omega}{k_z^{eff}} \approx \frac{\omega_p}{k_\perp}\left(1 + \frac{3}{2}\left(\frac{\bar{v}}{v_\phi}\right)^2\right). \tag{3.5}$$

where $1/k_\perp \approx R_P\sqrt{\frac{1}{2}\ln(R_w/R_p)}$ as before. For the modes studied here, $v_\phi/\bar{v} \gtrsim 3$ (thus $(\bar{v}/v_\phi)^2 \lesssim 0.1$), we see that the phase velocity v_ϕ is only weakly dependent on the plasma temperature or wavenumber k_z. In order to vary the damping rate, we heat the plasma. This changes $\bar{v}$ at roughly constant v_ϕ, enabling a comparison to Equation 3.4. The slight temperature dependence of the phase velocity is accounted for in the estimates of $v_\phi/\bar{v}$ by using the measured mode frequency to calculate the phase velocity at each temperature.

The same "Driftk" code that was used to calculate the mode dispersion $\omega(k_z^{eff})$ is used to calculate the theoretical damping rate. The numerical code includes the full (non-approximate) plasma dispersion function for a Maxwellian velocity distribution, and thus includes the temperature corrections to high order.

One limitation is that the code is only 1-D (radial), with the plasma assumed to be infinite in z with a prescribed k_z as discussed in Section 3.2. Further, the code assumes a single temperature for the whole plasma. Any radial variation in the temperature would cause a radial variation to the damping rate which is not accounted for; however, these corrections are assumed to be small.

3.3.2 Linear vs. Nonlinear

The damping of the mode can be nonlinear even though the mode is in the "linear regime"; essentially, the mode is linear because $\delta n/n \ll 1$, but the damping is nonlinear because the population of resonant electrons is strongly perturbed. The Vlasov equation for the distribution function $f(v)$ has a natural ordering for amplitude as discussed by O'Neil in 1965 [4]. When the perturbation to the distribution function f_1 becomes of the same order as the velocity perturbation of the resonant electrons δv, the linear approximation breaks down. This sets an upper amplitude limit to linear Landau damping. To see this limit, we solve the linearized equation for the perturbation to the distribution function.

Starting with the 1-D Vlasov equation,

$$\frac{\partial f}{\partial t} + v\frac{\partial f}{\partial z} - \frac{eE_z}{m}\frac{\partial f}{\partial v} = 0. \tag{3.6}$$

we find the linear solution by substituting $f = f_0 + f_1$, where $f_1 \sim e^{-i\omega t + ik_z z}$ is the perturbation to the distribution function, and f_0 is the unperturbed distribution, independent of time and homogeneous in space. Assuming $\partial f_1/\partial v \ll \partial f_0/\partial v$, we obtain

$$f_1 = i\frac{eE_z}{m}\frac{1}{\omega - kv}\frac{\partial f_0}{\partial v}. \tag{3.7}$$

Now, to check the limit to the above assumption, we calculate $\partial f_1/\partial v$ near the wave phase velocity $v_\phi = \omega/k$. Using $\omega_T^2 \equiv eE_z k_z/m$, and noting that for $v \sim v_\phi$ and $\gamma/\omega \ll 1$, $\omega - k_z v \approx \omega_0 + i\gamma - k_z v \approx i\gamma$, we find

$$\frac{\partial f_1}{\partial v}|_{v_\phi} \sim \frac{\omega_T^2}{\gamma^2}\frac{\partial f_0}{\partial v}|_{v_\phi} + \ \ldots \ O\left(\frac{1}{\gamma}\right). \tag{3.8}$$

It is easy to see that when $\omega_T \sim \gamma_L$, the assumption that $\partial f_1/\partial v \ll \partial f_0/\partial v$, is no longer true and the linear solution will fail. From a dynamical point of view, this means that electrons near the phase velocity will become trapped by the wave, causing a strong perturbation to their orbits, and dramatically modifying the damping of the wave. This breakdown of the linear theory and the nonlinear trapping of electrons by the wave is discussed and verified in Chapter 4.

Another limit is set by the number of particles available to Landau damp the wave. When the phase velocity is high (or thermal velocity low), the resonance will be far into the tail of the distribution. We can estimate the number of particles in the linear mode resonance, by integrating the distribution near the wave phase velocity with a width determined by the linear damping rate ($\Delta v = 2\gamma_L/k_z \ll \bar{v}$),

$$N_{res} = Q_{tot}\int_{v_\phi-\gamma_L/k_z}^{v_\phi+\gamma_L/k_z} dv\ f_0 \approx\ f_0\,\frac{2\gamma_L}{k_z}\,Q_{tot}\ \approx\ \frac{1}{2}\left(\frac{v_\phi}{\bar{v}}\right)^4 \exp\left[-\left(\frac{v_\phi}{\bar{v}}\right)^2\right]\,Q_{tot}. \tag{3.9}$$

Assuming a plasma with $Q_{tot} = 10^9$ electrons, Equation 3.9 says that there are only about 6 electrons in a linear resonance width for a wave with $v_\phi/\bar{v} = 5$. This sets another natural ordering for our trapped plasmas. If the plasma only had $Q_{tot} = 10^8$, then the same wave would only have 0.6 electrons in the linear resonance, and thus no linear Landau damping would be expected.

3.4 Linear Damping Measurements

Taking data only in the linear regime and varying the temperature we are able to check the theory of Landau. A summary of the data, γ_L/ω as a function of

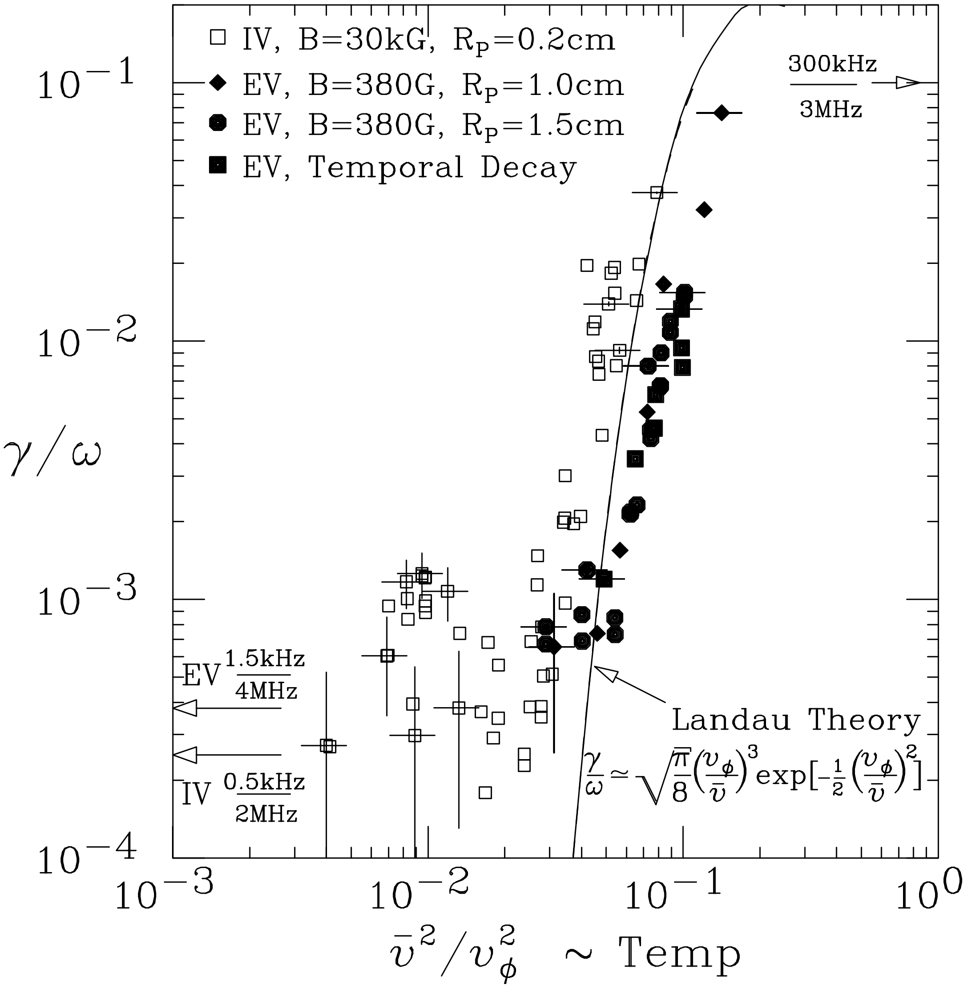

Figure 3.4: Linear damping rate compared to theory of Landau.

$\bar{v}^2/v_\phi^2$, is shown in Figure 3.4. Normalizing the temperature (as $\bar{v}^2 = T/m$) with the wave phase velocity enables a comparison between different traps and different plasma parameters (different v_ϕ). Over the range of parameters where Landau damping is expected to dominate, we see good quantitative agreement (within a factor of 2) with the absolute theory of Landau. This close agreement between experiments on two machines (EV and IV), using two measurement techniques (spectral and temporal), with the theory of linear Landau damping in the range $3 < v_\phi/\bar{v} < 5$ as seen in Figure 3.4, is the first main result from this thesis.

At low temperatures where collisionless damping is expected to be negligible we see a finite amount of damping which is roughly independent of temperature. The measured residual damping in this regime is due to either resistive dissipation from the amplifier input impedance or the limit of the measurement of mode widths as discussed in Section 2.3. This frequency dependent limit for different bandwidth receivers is labeled in Figure 3.4 with arrows.

3.4.1 Thermal Mode Experiments

Measurements of the spectral width of thermally excited T-G waves have been made on trapped pure electron plasmas [30, 15]. Thermal electrons are constantly emitting and absorbing waves. This process of emission and absorption can be viewed as random kicks leading to the excitation of coherent plasma oscillations even when there is no external drive applied.

These small amplitude modes are most readily identified by decreasing V_{exc} to zero, as shown in Figure 3.5 where 3 broad spectrum scans of received amplitude versus frequency for -80dBm, -100dBm, and no drive, respectively. As can be seen in Scan (c), the peaks at the mode frequencies still exist even when no drive is present.

A close up of the lowest frequency ($m_z = 1$) mode at 4 different temperatures is shown in Figure 3.6. Generally, as the temperature increases, the measured mode width (ie. damping) increases and the peak amplitude decreases. This is consistent with the simple harmonic oscillator picture described in Section 2.3.3 ($V_m \propto 1/\gamma$).

Further, the energy in the mode (the area under the curve) has been measured and shown to be proportional to the plasma temperature [30]. Lastly, the curve at the lowest temperature (.06eV) appears qualitatively different than the

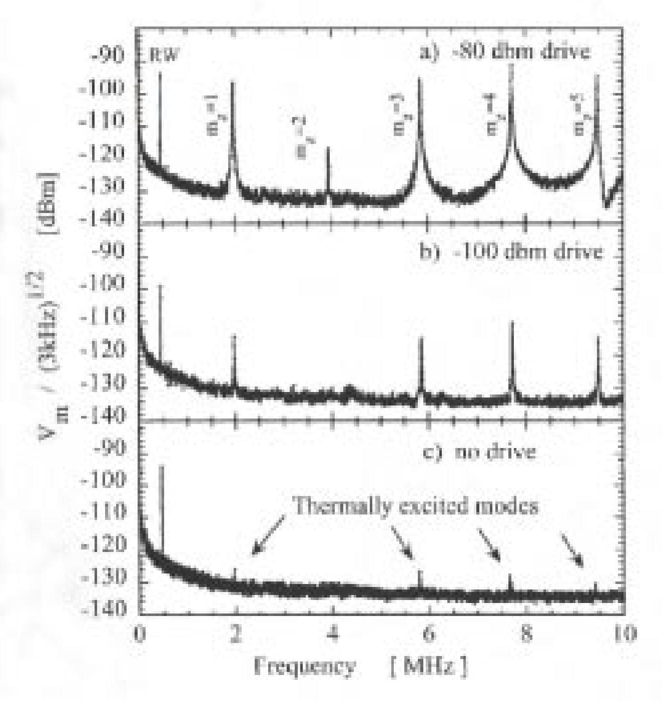

Figure 3.5: Thermal spectrum measurement.

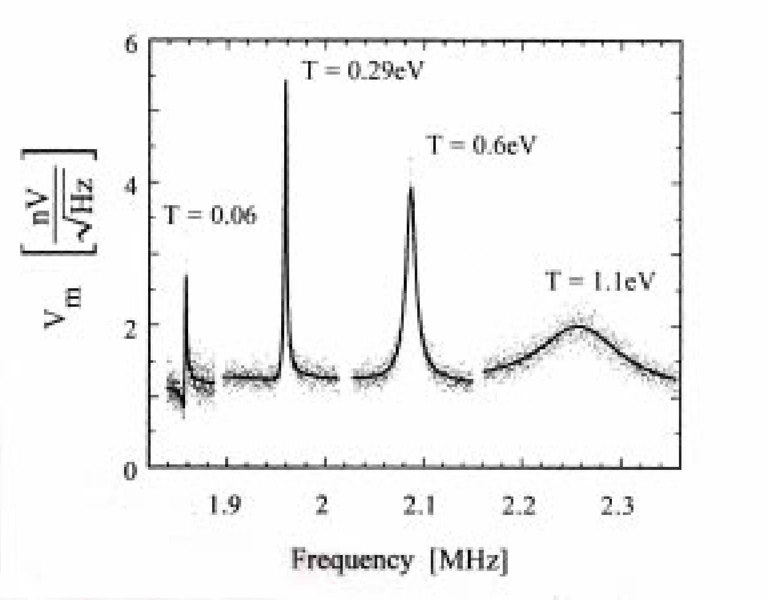

Figure 3.6: Thermal spectrum with fits.

others. This is because the low-temperature plasma is an absorber of noise generated in the amplifier circuit. In this regime, the resonance shape of the detected spectrum is significantly influenced by the impedance and temperature of the detection circuit [30].

The mode damping rates obtained from measured thermal spectrum widths are plotted in Figure 3.4 as hollow squares for the IV experiments and solid diamonds and circles for the EV experiments.

3.4.2 Temporal Decay Experiments

The temporal evolution of launched waves elucidates both the linear damping process and the nonlinear trapping oscillations to be discussed in Chapter 4. In this case, the damping rate is extracted from the measured exponential decay of the mode after being linearly excited for a fixed number of cycles [26, 31].

One such measurement is shown in Figure 3.7, where the excitation is 10 cyles long. The received amplitude from the fixed frequency spectrum analyzer, with bandwidth $BW = 300$kHz, is plotted as a function of time on a logarithmic scale, so a straight line signifies exponential decay. For small V_{exc}, the wave is observed to damp exponentially at a rate independent of amplitude. As the amplitude is increased, oscillations in the amplitude develop and halt the decay of the wave. These oscillations are due to trapping of the resonant electrons in the wave potential, and are discussed in detail in Chapter 4. Even with the amplitude oscillations, the initial decay rate can be seen to be identical to that of the the low amplitude decay. This means that the same fast initial damping occurs at both low and high amplitudes

Taking data only from the early part of the evolution (the fast initial damping) and varying the temperature we are able to check the theory of Landau. One

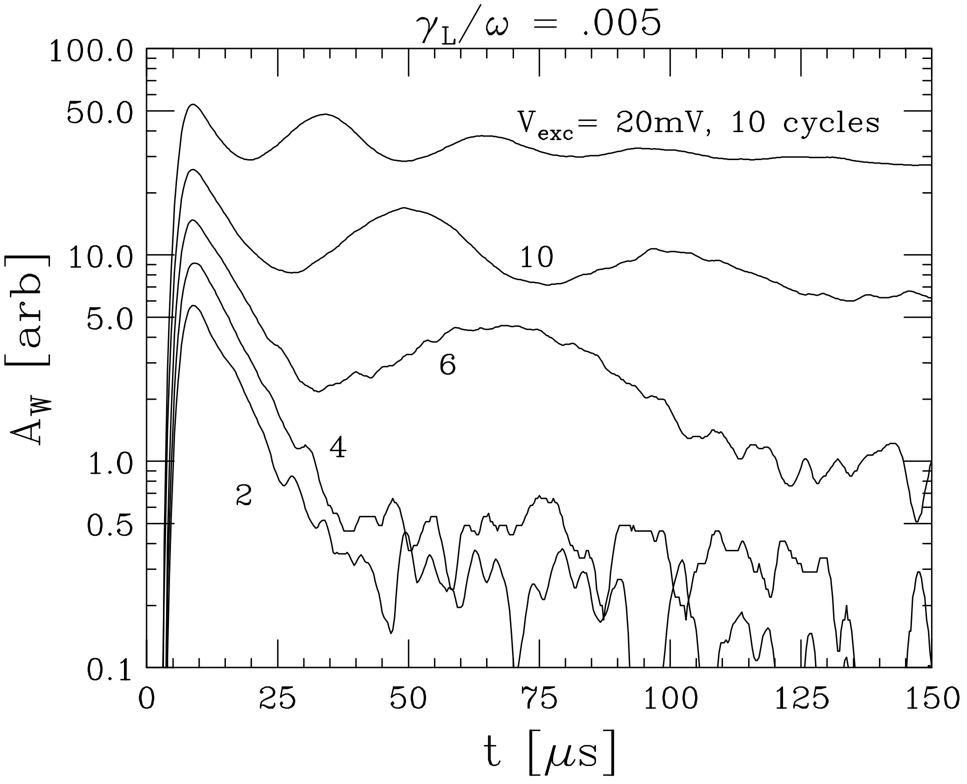

Figure 3.7: Recorded waveforms from the pulse-decay experiment.

set of temporal damping data taken on EV is shown in Figure 3.4 as solid squares. The measured linear damping rate is approximately the same using either temporal decay or spectral width (solid circles) to measure γ_L.

3.4.3 Verification of the Landau Resonance

We have verified experimentally that the observed Landau damping arises from resonant electrons with axial velocity equal to the wave phase velocity, ie. $v \approx v_\phi = \omega/k_z$; by eliminating these electrons, the observed damping decreases by a factor of 10. Since the damping depends on the slope of the distribution at the resonant velocity v_ϕ, modifying the number of particles near this velocity has a strong impact on the damping rate.

The experiment uses the technique of plasma "hollowing" which has been

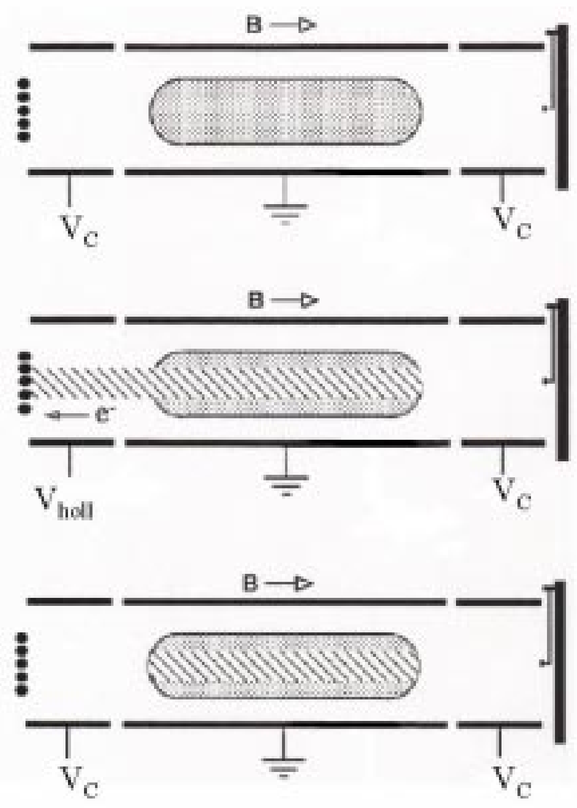

Figure 3.8: Fast electrons are ejected during hollowing of the column.

used to study the diocotron instability in hollow electron columns [32]. If one of the confinement voltages is lowered toward the plasma potential, the most energetic electrons are able to escape out of the confinement region as showing pictorially in Figure 3.8. If the hollowing process is slow compared to the thermal electron bounce frequency, then all electrons above a certain energy (which varies with radius) will escape, effectively eliminating the high energy tail of the initial Maxwellian (shown pictorially in Figure 3.9). The hollowing has to be done faster than the unstable diocotron wave growth time to avoid bulk radial transport of particles. Moreover, if the hollowing is too deep, then the total charge in the plasma will change significantly and the mode frequency will change. All the experiments described here used only slight hollowing, with $\delta Q_{tot}/Q_{tot} < 2\%$. Note that for a

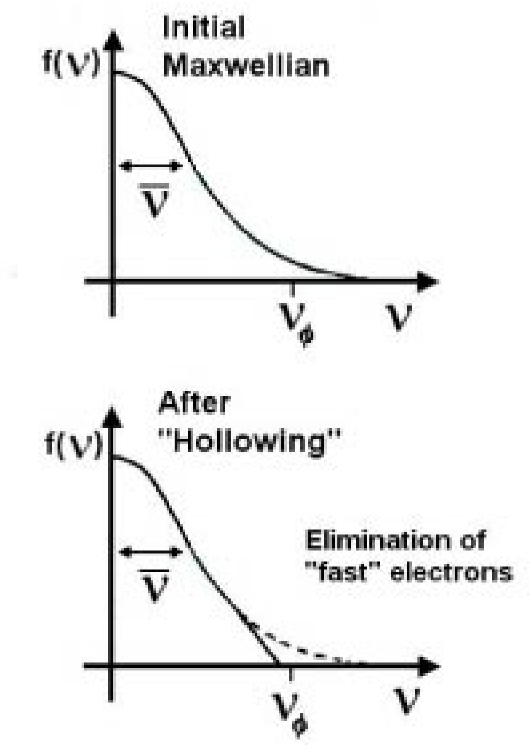

Figure 3.9: High energy tail of the distribution function is removed after hollowing process.

Maxwellian, the percentage of electrons with velocities greater than $3\bar{v}$ is $\sim 2\%$, so we can modify the damping for all weakly damped waves ($v_\phi > 3\bar{v}$) without significantly altering the frequency of the wave.

The suppression of wave damping when hollowing progressively eliminates the resonant electrons is shown in Figure 3.10. With no hollowing, a short sinusoidal burst excites a T-G wave with clear Landau damping and a single amplitude oscillation (similar to the 6mV wave in Figure 3.7). For weak hollowing (such as the $V_{holl} - 40$V curve), the damping is not modified significantly. However, for $V_{holl} < -36$V, the slope of the initial decay is seen to decrease (and the amplitude of the oscillation increases). This decrease of damping as the hollowing gets deeper continues until the fast (Landau) damping is eliminated and only damping due to

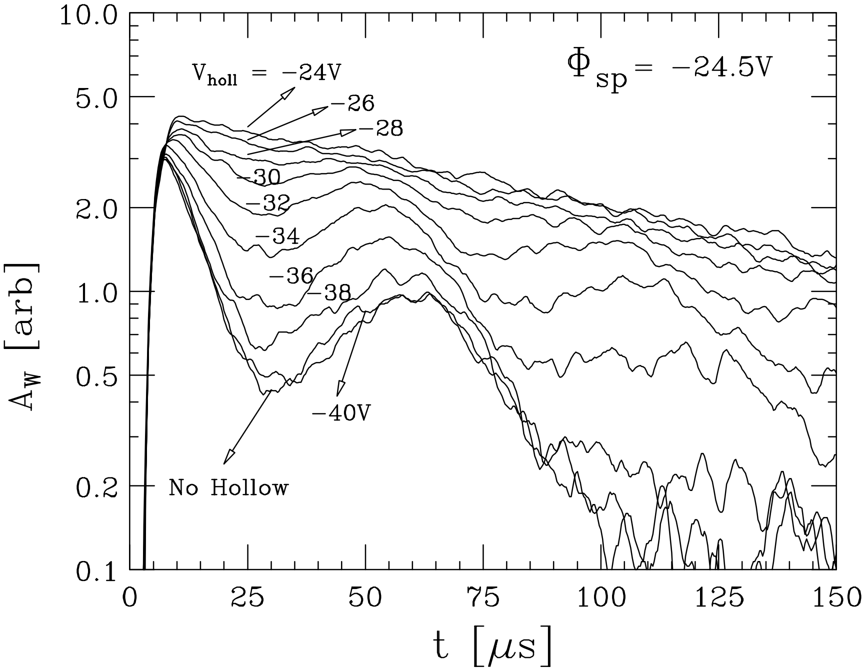

Figure 3.10: Plots of damping after hollowing.

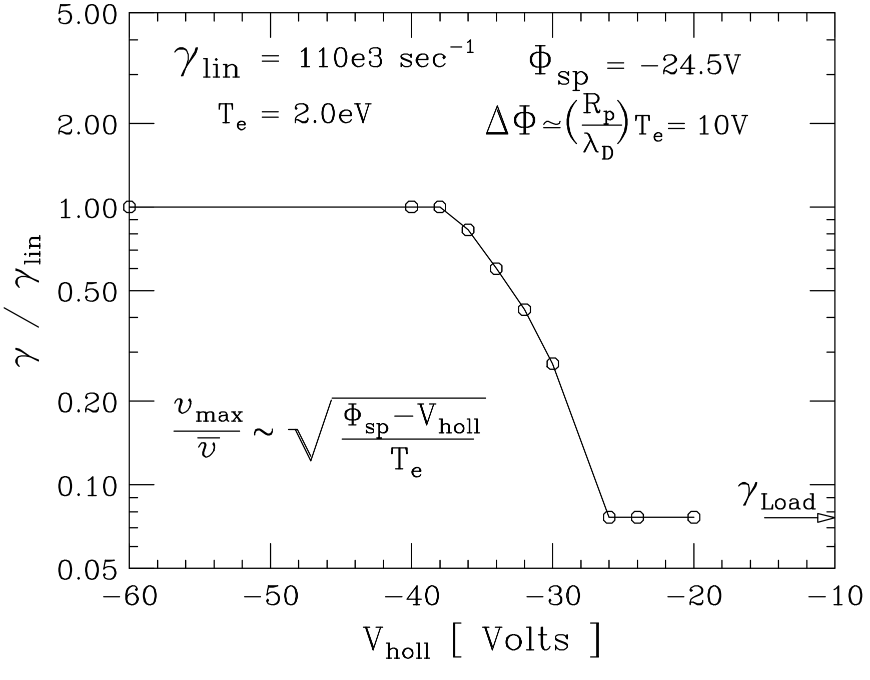

Figure 3.11: Measured effective damping rate versus hollow level.

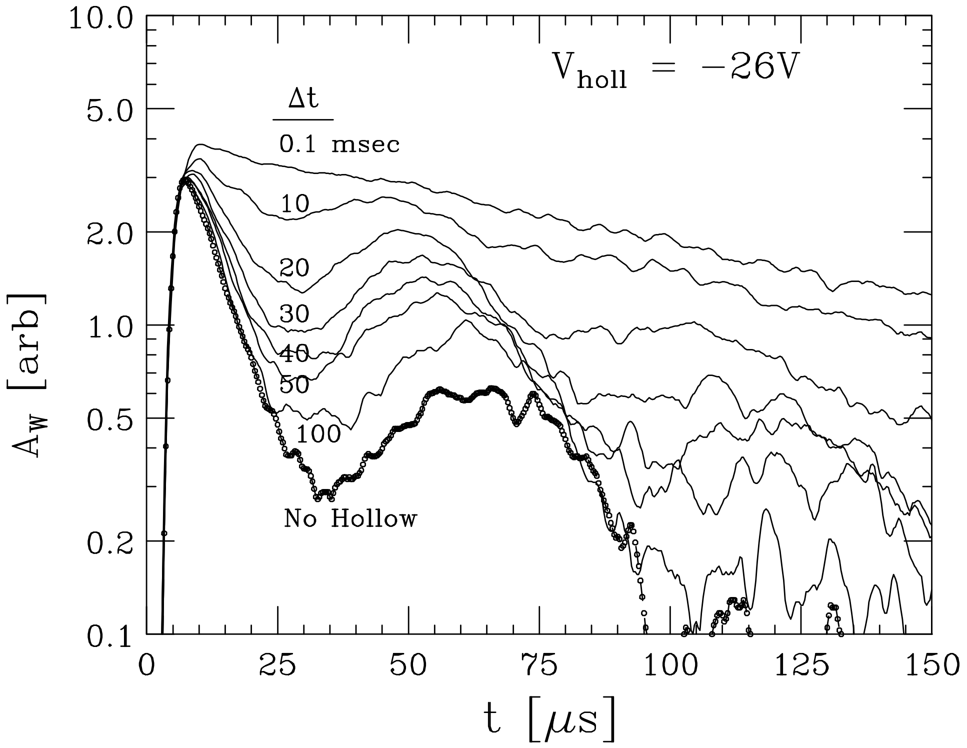

Figure 3.12: Relaxation of damping back to Landau after hollowing to -26V.

the resistive impedence of the detection circuit is left. Further, the amplitude oscillation is observed to be eliminated as well, demonstrating that these oscillations are also dependent on the resonant electrons.

The measured initial damping rate for this data set is shown in Figure 3.11. For weak hollowing, the damping rate is unaffected; but as the hollowing is increased, the damping rate is modified dramatically. When all resonant electrons are removed, the fast initial wave damping is totally eliminated and the wave is dominated by the resistive damping from the measurement circuit.

We argue that the hollowing process only eliminates the fast particles and leaves the rest of the plasma alone. If the plasma is not substantially changed (density and bulk temperature) then collisions should eventually re-populate the tail of the distribution function. Figure 3.12 shows damped waves for different delay times Δt between the hollowing and the wave excitation as well as the received signal for a wave with no hollowing. The original resonant Landau damping and trapping oscillation are observed to re-appear in about 20msec after hollowing, as electron-electron collisions re-populate the resonant electron velocities.

As mentioned above, previous experiments have shown that hollow levels with $\Delta Q_{tot}/Q_{tot} \gg 1\%$ are unstable to diocotron mode growth [33]. This instability also causes large levels of turbulent cross-magnetic field transport [34]. Future wave damping experiments on hollow columns can measure the turbulent transport rate of edge electrons into the center of the column by finding the time delay necessary for significant Landau damping to appear.

3.5 Bounce Resonances and Sheath Damping

Surprisingly, the experimental results of Section 3.4 show no correspondence to the theoretical predictions of “bounce resonant harmonic damping” and “sheath damping,” both having to do with the finite length of the system. Bounce resonant harmonic damping is an enhancement to Landau damping from the coupling of the standing wave to harmonics of the electron bounce motion. Here the bounce motion refers to the reflection (or “bouncing”) of the electrons between the ends of the column; this contrasts to the nonlinear “amplitude bounces” discussed in Chapter 4. Sheath damping is the destruction of coherent velocity perturbations due to the finite electron penetration time in the end sheaths, causing the energy in the standing wave to be converted to random thermal motion.

3.5.1 Bounce Resonant Damping

An analysis of the true mode potential in terms of the plasma length L_p gives rise to a sum over all the bounce harmonics of the electron motion. This is

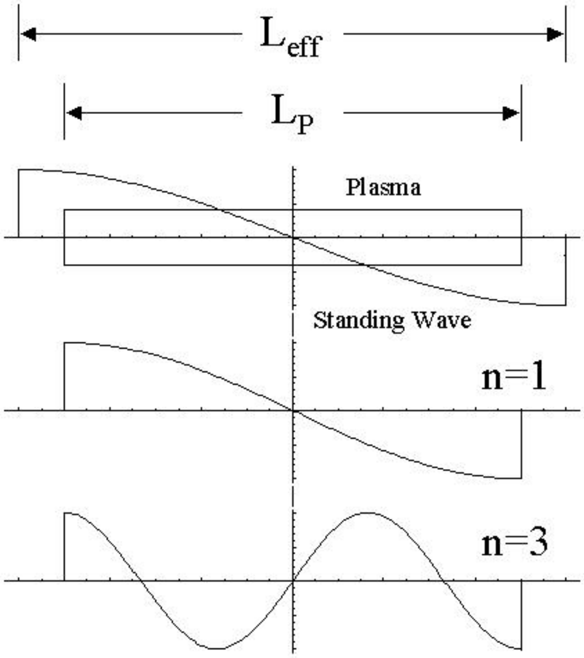

Figure 3.13: Physical picture of the bounce resonant coupling model.

similar to trying to match a long wavelength mode into a smaller box. The wave will not exactly match any mode of the box, but rather will be made up of many harmonics, with each harmonic contributing to the damping rate [35], similar to effects seen in magetic-mirror confined plasmas [36].

To calculate the total bounce resonant damping rate γ_{BRD} we use a simple plasma model with flat ends [37]. We assume that each harmonic n will contribute a damping γ_n as expected from linear Landau theory, except that each will have a different phase velocity (of v_ϕ/n) and coupling coefficient $\mathcal{F}_n$. We obtain the coupling coefficient for each mode by calculating the Fourier transform of the mode with $k = \pi/L_{eff}$ to modes with $k = n\pi/L_p$, as shown pictorially in Figure 3.13. As discussed in Section 3.2, numerical simulations have shown that a good approx-

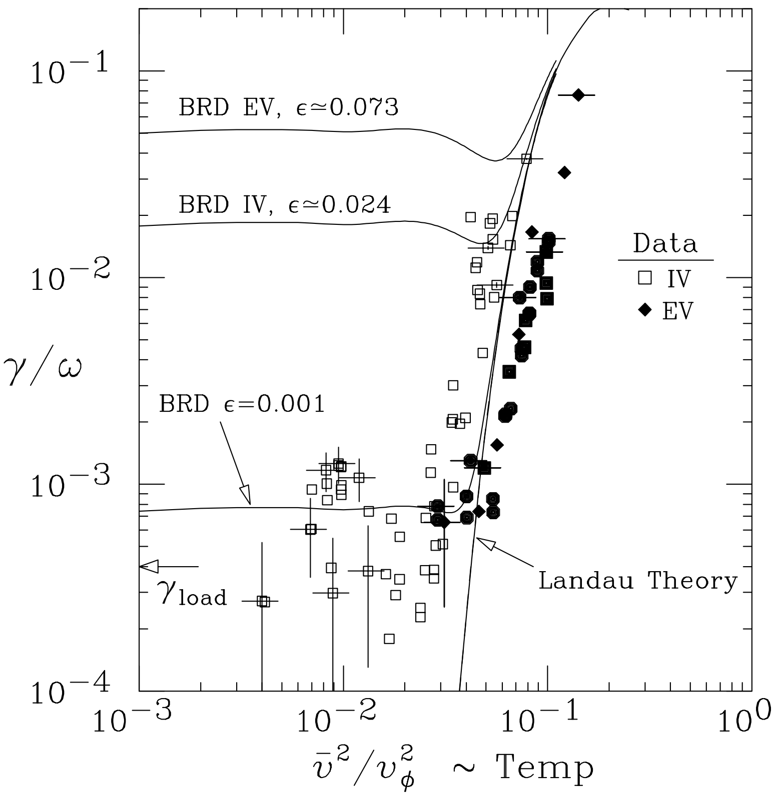

Figure 3.14: Comparison of the measured linear damping rate to a simple estimate of Bounce Resonant Harmonic Damping (BRD). The theory depends on $\epsilon = \delta L/L$ and is evaluated for EV and IV.

imation for L_{eff} when $R_P/L_P \ll 1$ is [25]

$$L_{eff} = L_p + 0.3R_w + 0.7R_p \equiv L_p(1+\epsilon). \tag{3.10}$$

Doing the algebra, we obtain:

$$\frac{\gamma_{BRD}}{\omega} = \sum_{n=odd} \frac{\gamma_n}{\omega}\,\mathcal{F}_n \tag{3.11}$$

$$\frac{\gamma_n}{\omega} \approx \sqrt{\frac{\pi}{8}}\left(\frac{v_\phi}{n\bar{v}}\right)^3 \exp\left[-\frac{1}{2}\left(\frac{v_\phi}{n\bar{v}}\right)^2\right] \tag{3.12}$$

$$\mathcal{F}_n = \frac{n}{n^2 - \left(\frac{L_p}{L_{eff}}\right)^2}\,\sin\left(\pi\frac{L_p}{L_{eff}}\right). \tag{3.13}$$

In Figure 3.14, the measured linear damping rate data is replotted along with the calculated enhanced bounce resonant damping rate BRD for EV ($R_p \approx 1.5\text{cm}, R_w = 3.81\text{cm}, L_p \approx 30\text{cm}, \epsilon \approx .073$) and IV ($R_p \approx 0.2\text{cm}, R_w = 2.86\text{cm}, L_p \approx 41\text{cm}, \epsilon \approx .024$). Also shown is a reference curve with $\epsilon = .001$ for comparison. The theory curves were derived from Equation 3.11 using a sum from $n = 1$ to $n = 51$. The number of harmonics is limited by collisions knocking the electrons out of resonance. For an effective collision frequency ν_{eff}/ω (see Section 3.5.2), this limit is

$$\frac{1}{n_m}\frac{v_\phi}{\bar{v}} = \frac{\nu_{eff}}{\omega} \tag{3.14}$$

which says that $n_m \gtrsim 300$, for $v_\phi/\bar{v} = 3$ and $\nu_{eff}/\omega \sim .01$. The theory calculation using $n_m = 101$ or $n_m = 151$ are identical to the curves for $n_m = 51$.

The damping data shows no correspondence with the bounce-resonance enhancement calculation assuming flat ends and using $\epsilon = (L_{eff} - L_p)/L_p$. However, the ends of the plasma are actually curved [38, 39], possibly making the effective ϵ smaller than used in our simple estimate. The reference curve shows that $\epsilon = .001$ is in qualitative agreement with the data; however this is more than an order of magnitude smaller than any estimate using flat ends. Here, the theory is constrained by the measured mode dispersion (see Section 3.2) which shows that L_{eff} is essentially given by Equation 3.10. Numerical simulations of wave propagation using realistic end-shapes might be able to obtain a better estimate for ϵ, so that we can make a quantitative comparison to the theory of bounce resonant harmonic damping.

3.5.2 Sheath Damping

The electron plasma has "sheaths" at the plasma ends, where the electrons interact with the confinement potentials and are reflected. This sheath region is about a Debye length (λ_D) in size [40]. This means that a thermal electron (with velocity $\bar{v}$) requires a time of about $\lambda_D/\bar{v} = 1/\omega_p$ to reflect off the ends of the plasma column.

Trivelpiece-Gould modes are electrostatic compression waves of the plasma column. These oscillations consist of the conversion of electrostatic (potential) energy (in the form of perturbed electron density δn) into mechanical (kinetic) energy (ie. $\frac{1}{2}m\delta v^2$), and vice-versa.

As shown by Bohm and Gross [41, 42], the presence of the wave perturbs the velocity of the electrons,

$$v_z = v_{z0} + \delta v_z \tag{3.15}$$

where δv_z is the coherent velocity perturbation for an electron with unperturbed velocity v_{z0}. For a standing plasma wave with potential $\phi = \phi_0 \left[e^{i(kz-\omega t)} + e^{-i(kz+\omega t)}\right]$, δv_z is given by

$$\delta v_z = \frac{ek\phi_0}{m}\frac{e^{i(kz-\omega t)}}{\omega - kv_{z0}} - \frac{ek\phi_0}{m}\frac{e^{-i(kz+\omega t)}}{\omega + kv_{z0}}. \tag{3.16}$$

Note that given $\phi \propto \cos(kz)$, we obtain a perturbed velocity with $\delta v_z \propto \sin(kz)$, ie. δv_z is 90 deg out of phase with ϕ, as expected for these compression waves.

Assuming that $v_{z0} \ll v_\phi$ (ignoring resonant electrons) Bohm and Gross found that the velocity perturbation at one end of the plasma (eg. z=0) is given by [43]

$$\delta v_z|_{z=0} \approx \frac{2e}{m\omega^2}k^2\, v_{z0}\, \phi_0 e^{-i\omega t}. \tag{3.17}$$

Further, the time average of the energy of the velocity perturbation is given by

$\langle \Delta E \rangle_{Av} = \frac{1}{2} m \langle (\delta v_z)^2 \rangle_{Av}$. Averaging this over all unperturbed velocities v_{z0} using a Maxwellian velocity distribution, gives the average change of energy per particle striking the end sheath as

$$[\langle \Delta E \rangle_{Av}] \approx \frac{1}{2} m \bar{v}^2 \left(\frac{e\phi_0 k^2}{m\omega^2} \right)^2 . \tag{3.18}$$

Because of the finite penetration time before reflection, Bohm and Gross concluded that the "velocity perturbation with which the particles strike the sheath will lose its coherence with the wave" [43]. This imperfect reflection causes a decoherence between the mechanical and electrostatic energy; some wave energy is converted into random thermal energy resulting in decay of the standing wave. Notice that in Equation 3.18, the energy per particle goes like the square of the wave amplitude. Since the energy in the wave also goes like the square of the wave amplitude, we see that the damping rate will be independent of wave amplitude.

Assuming that there is complete loss of coherence at the sheath and noting that the current of particles striking the end sheaths is given by [43]

$$j = 2 \left(\frac{1}{\sqrt{2\pi}} \right) \bar{v} n_0 \, \pi R_p^2, \tag{3.19}$$

the damping rate from sheath decoherence for standing T-G waves is given by

$$\frac{\gamma_{sheath}}{\omega} = \left(\frac{8}{\pi} \frac{3}{\sqrt{2\pi}} \right) \left(\frac{\omega_p}{\omega} \frac{k_z}{k_\perp} \right)^2 \left(\frac{\bar{v}}{v_\phi} \right)^3 \approx 3.05 \left(\frac{\bar{v}}{v_\phi} \right)^3 . \tag{3.20}$$

In Equation 3.20 we made use of the approximate mode dispersion, $\omega/\omega_p \approx k_z/k_\perp$, from Equation 3.1.

Figure 3.15 replots the linear damping rate measurements along with the prediction for sheath damping given by Equation 3.20. The estimate of sheath damping (dashed curve) predicts an enhanced damping rate over the Landau rate

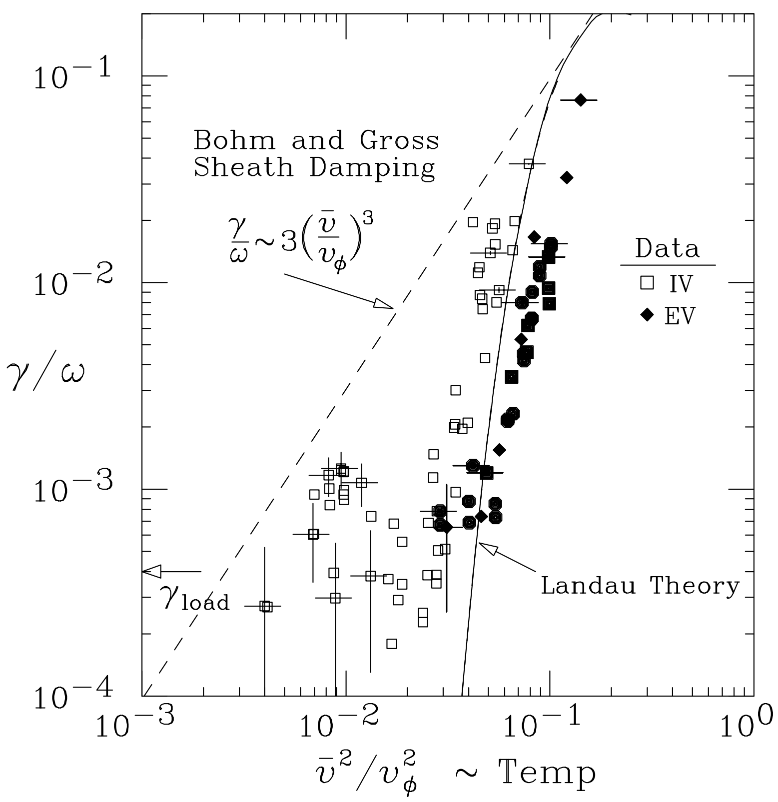

Figure 3.15: Measured damping rate compared to sheath damping as predicted by Bohm and Gross.

(solid curve). This simple estimate disagrees with the data by as much as a factor of 10.

This disagreement is not totally unexpected. The theory assumes that there is a total loss of coherence of the velocity perturbation when electrons penetrate the end sheath. This will be correct if the penetration time is close to the wave period (or $\omega_{wave} \sim \omega_p$), implying the wave has dramatically changed its phase by the time the electron has been reflected. However, in the experiments, $\omega_{wave} \approx 0.1\omega_p$, so the electrons reflect on a time scale much shorter than the the wave period. This means that the electrons are still mostly in phase with the wave and we expect the dissipation to be less than predicted by theory.

Future experiments using shorter plasma lengths (with higher mode frequencies) would better satisfy the approximations used by Bohm and Gross, and might show the signature of sheath damping.

Chapter 4

Nonlinear Trapping Oscillations

4.1 Overview

Large amplitude waves trap the resonant electron population before the wave has time to damp. As described in the previous section, this is a fundamental limit to Landau damping. The classic picture is that the resonant electrons become trapped during a time $1/\omega_T = \sqrt{m/eE_z k_z}$, picking up enough energy to overtake the wave. When they try to overtake the wave, the wave potential now causes the electrons to lose energy and give it back to the wave, and the cycle continues [4]. Thus, as the electrons bounce back and forth inside of the potential well of the wave, the wave periodically grows and damps. Since the initial phase of the electrons entering the potential well is random, eventually the electrons will phase mix and the amplitude of the wave becomes constant with time. This is the classic development of what is referred to as a BGK equilibria [44], a topic that is still being debated [45, 46, 47].

This chapter presents O'Neil's theory of these trapping oscillations, including a simple numerical treatment to avoid some of the approximations used in the theory. Detailed experiments verifying this trapping process in trapped pure electron plasmas are presented. Measurements of the time of the first trapping oscillation are in very good agreement with the absolute predictions of the numerical calculations (and the classic theory in the appropriate limit). To my knowledge, these are the first measurements of temporal trapping to be compared to absolute predictions of the nonlinear theory with no adjustable parameters. Small discrepancies in bounce oscillations at low amplitude are observed; this is likely a result of extra damping not accounted for in the theory. Further, measurements of the average (nonlinear) decay rate of the mode is shown to be consistent with collisional repopulation of the resonant particles. This chapter concludes with a comparison of the measured effective plateau amplitude to the amplitude predicted for a "BGK equilibrium."

4.2 Theory

4.2.1 O'Neil's Work ($1 \ll \omega_T/\gamma_L$)

O'Neil solved for the exact nonlinear dynamics of trapped resonant electrons in a prescribed wave potential. He assumed that the amplitude is large enough so that no significant damping takes place before the trapping time. For the untrapped (non-resonant) electrons, he solved the linearized Vlasov equation. This theory is ostensibly applicable as long as the trapping oscillations at ω_T develop in a time short compared to the linear Landau damping rate γ_L, ie. $\omega_T \gg \gamma_L$.

O'Neil used elliptic integrals to solve for the exact orbit of the resonant electrons in the stationary potential well of the plasma wave. He then calculates the work done by the particles in executing their trapped orbits and uses conservation of energy to derive the dynamics of the wave. For the case of a simple one-dimensional, infinite, homogeneous plasma with a single sinusoidal plane wave, O'Neil derived [4]

$$\gamma(t) = \gamma_L \sum_{n=0}^{\infty} 64\pi \mathcal{J}_n(t) \tag{4.1}$$

$$\mathcal{J}_n(t) = \int d\kappa \left\{ \frac{2n \sin\left(\frac{n\pi t\omega_T}{\kappa F}\right)}{\kappa^5 F^2(1+q^{2n})(1+q^{-2n})} + \frac{(2n+1)\sin\left(\frac{(2n+1)\pi t\omega_T}{2F}\right)}{F^2(1+q^{2n+1})(1+q^{-2n-1})} \right\} \tag{4.2}$$

where γ_L is the Landau damping rate from Equation 3.4, $F \equiv F[\kappa, \pi/2]$ is the complete elliptic integral of the first kind, $F' \equiv F[(1-\kappa^2)^{1/2}, \pi/2]$, and $q \equiv e^{\pi F'/F}$.

Further, the wave amplitude as a function of time defined by

$$\frac{\Phi(t)}{\Phi_0} \equiv \exp\left[-\int_0^t dt'\gamma(t')\right] \tag{4.3}$$

can be solved numerically for a given value of ω_T/γ_{LD}. Figure 4.1 gives the predicted wave amplitude (at r=0) versus time normalized to ω_T, for different values of ω_T/γ_L. The figure shows that the time for the oscillations to occur is inversely proportional to ω_T and that the height of the oscillations drops as ω_T/γ_L decreases. The phase mixing of the electron orbits and the evolution to a constant amplitude (BGK) state as $t \to \infty$ is also apparent.

4.2.2 Self-Consistent Numerical Calculations ($1 \leq \omega_T/\gamma_L$)

O'Neil's approximation of constant amplitude neglects many details about how the particles interact with the wave during the initial damping. For instance, it is obvious in Figure 4.1 that for $\omega_T/\gamma_L < 10$ there is significant damping before the oscillation occurs. A self-consistent treatment is necessary in order to obtain the behavior of the wave for $\gamma_L \sim \omega_T$. A consistent numerical solution is found by iteration of O'Neil's equations, as done by Oei and Swanson in Reference [48].

From the definition of the trapping frequency, $\omega_T \equiv \sqrt{ek^2\Phi_0/m}$, we can define a time dependent trapping frequency as

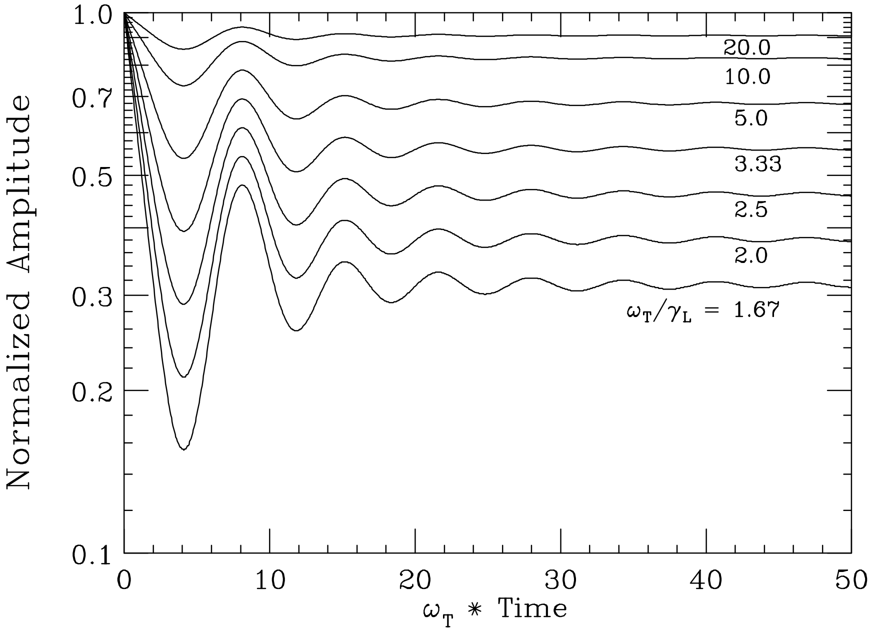

Figure 4.1: Temporal evolution of the wave potential as predicted by the theory of O'Neil, assuming $\omega_T \gg \gamma_L$.

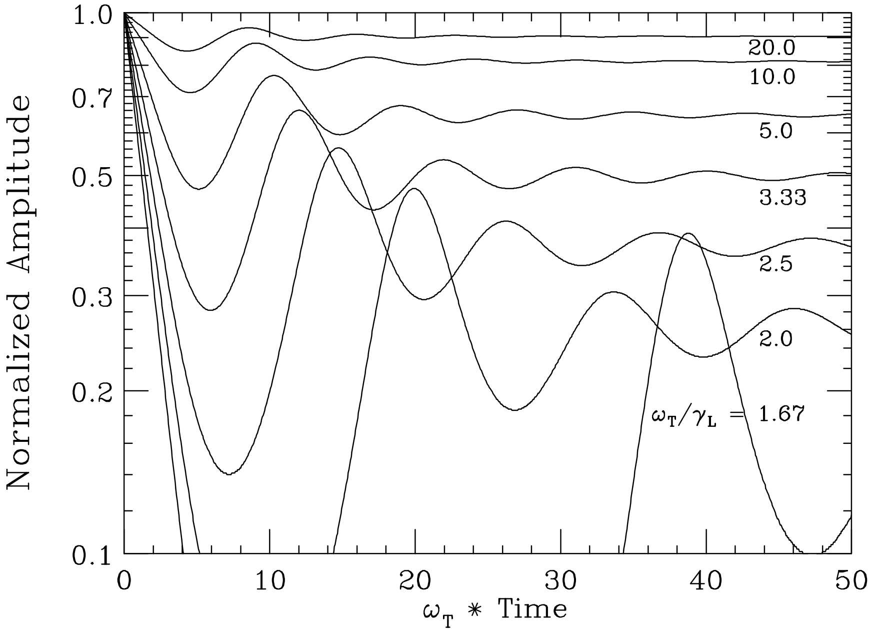

Figure 4.2: Temporal evolution of the wave potential as predicted by the numerical self-consistent caculations for $\omega_T > \gamma_L$.

$$\omega_T(t) \equiv \sqrt{\frac{ek^2\Phi(t)}{m}} = \omega_T \sqrt{\frac{\Phi(t)}{\Phi_0}} \,. \qquad (4.4)$$

For a given ω_T/γ_L, we first solve Equation 4.3 using $\gamma(t)$ from Equation 4.1, assuming that ω_T is fixed. Next, the time dependent trapping frequency is found from Equation 4.4. This calculated trapping frequency is used in Equation 4.1 and Equation 4.2 to find a new $\gamma(t)$, which is then used in Equation 4.3 to find the iterated $\Phi(t)$, and the process is repeated until the solution converges (typically 4 or 5 iterations).

This solution will be valid as long as significant loss (de-trapping) of resonant particles does not take place. Several authors have done numerical simulations to predict when the effect of de-trapping becomes important [49, 50]. Denavit, for example, predicts that no trapping oscillations will appear when $\omega_T/\gamma_L \lesssim 1.7$. This agrees within a factor of 2 to the limit observed in the experiments $\omega_T/\gamma_L \lesssim 2.6$.

Figure 4.2 plots the wave amplitude (at r=0) versus time normalized to ω_T, for different values of ω_T/γ_L as predicted by the self-consistent numerical calculation. Figure 4.2 shows that as ω_T/γ_L decreases, the time it takes for the first oscillation to develop increases. As before, there is significant damping of the wave before trapping for amplitudes with $\omega_T/\gamma_L < 10$. Not surprisingly, the figure also shows that the amplitude of the oscillations is smaller than the corresponding curve from Figure 4.1 due to the delay in the trapping process. Note that the subsequent oscillations that occur after the initial trapping do not have the same delay, since no further damping takes place after the resonant electrons become trapped. The phase mixing of the electron orbits and the evolution to a constant amplitude wave (ie. "BGK state") as $t \to \infty$ is also observed, but the plateau is at a level lower than that seen in Figure 4.1.

In the experiments, there is a radial profile for the mode potential and thus a

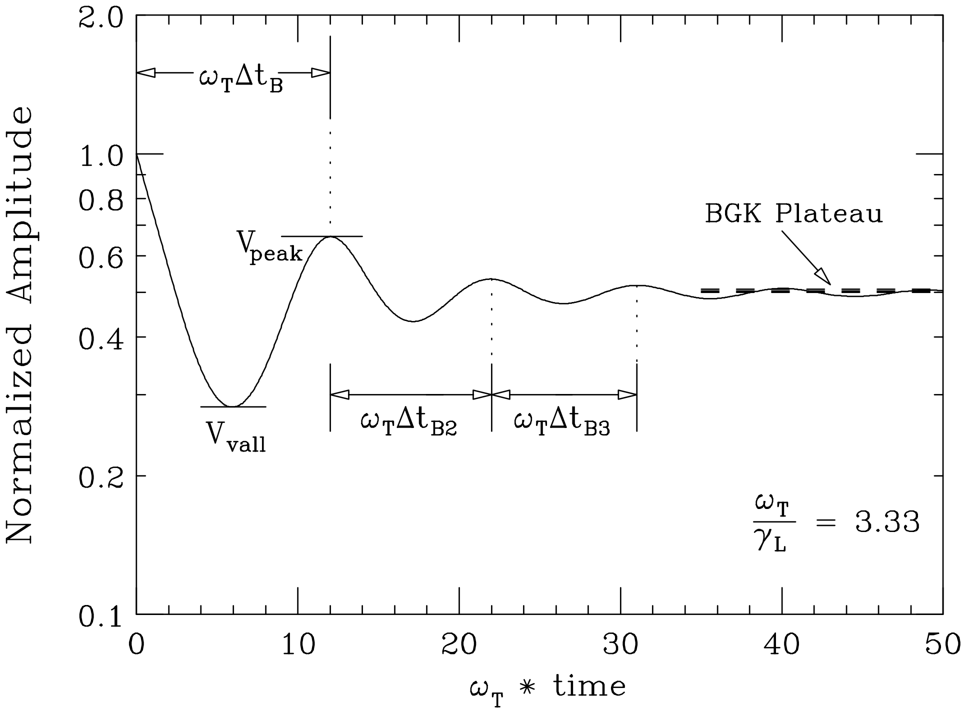

Figure 4.3: ω_B is defined as 2π times the inverse of the time between the peak of the wave amplitude and the peak of first oscillation (Δt_B). The "BGK" plateau develops as $t \rightarrow \infty$.

radial profile to the trapping frequency. The effect of the radial profile is estimated by performing a radial average over the eigenmode [51]. For the experimental profiles, this effect predicts a 10% drop in the expected trapping frequency due to the phase mixing of electrons at different radii with different wave potential.

4.2.3 ω_T vs. ω_B

In order to compare to the experiments we need to figure out what to measure. O'Neil's theory and the numerical solutions show that the time to the first peak in the wave amplitude is a well defined parameter, meaning that it is unique for each value of ω_T/γ_L. We call this the trapped particle "bounce" time (Δt_B), and the corresponding frequency is denoted $\omega_B \equiv 2\pi/\Delta t_B$, as shown in Figure 4.3. Later amplitude peaks occur in time increments of Δt_{Bn}, giving

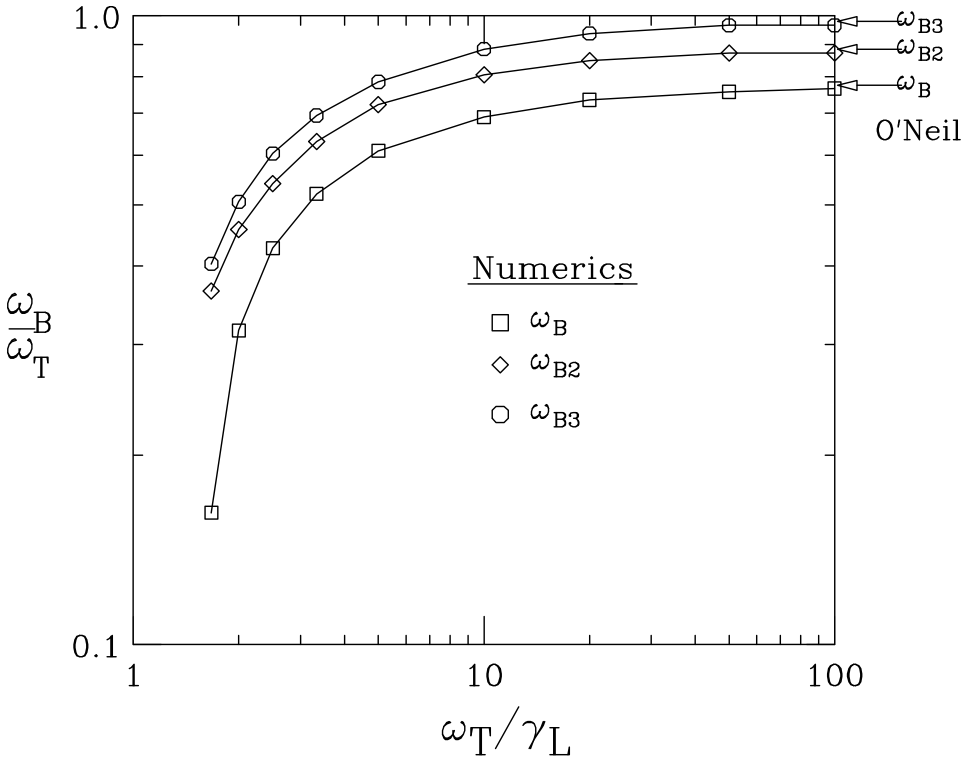

Figure 4.4: Predicted values of ω_B/ω_T from the self-consistent calculations for the first 3 bounce oscillations. Note that for $\omega_T/\gamma_L \gg 1$ the numerics plateau to O'Neil's values. Also note that as the bounce number gets large, $\omega_B \to \omega_T$.

frequencies $\omega_{Bn} \equiv 2\pi/\Delta t_{Bn}$.

In O'Neil's theory, $\omega_B \approx (2\pi/8)\omega_T$ for all ω_T/γ_L (Figure 4.1). The self-consistent numerics modify the time of the first amplitude peak for wave amplitudes where $\omega_T/\gamma_L < 10$, but identical times for $\omega_T/\gamma_L > 10$. Figure 4.4 plots the bounce frequencies for the first 3 trapping oscillations as obtained from Figure 4.2 and indicates the values predicted by O'Neil (from Figure 4.1) by arrows.

4.3 Experiments

4.3.1 Measurement of ω_B

In the plots to be presented, the theory curve predicted from the numerical solution will be shown as a solid line, and the theory curve predicted from O'Neil's theory will be shown as a dashed line.

The experiments use a short burst (typically 10 cycles) to excite a T-G wave; the decay of the wave is measured by the charge amplifier as described in Section 2.3, so as to minimize resistive damping of the wave.

Raw data from a large amplitude wave decay experiment on EV with a warm plasma (temperature ≈ 2.5 eV) is shown in Figure 4.5. Here the measured wave potential at the wall is shown as a function of time for waves of different initial amplitudes. The trapping oscillations are easily seen, and ω_B is obtained directly from the plots (eg. Figure 4.6). Using the calibration procedure described in Section 2.4, we use the peak received wave amplitude to calculate E_{z0}; where E_{z0} is the initial wave amplitude at $r = 0$. Using E_{z0}, an estimate of the basic trapping frequency ω_T is obtained from $\omega_T^{(E)} \equiv \sqrt{eE_{z0}k_z/m}$.

Figure 4.7 shows the measured amplitude bounce frequency $\omega_B = 2\pi/\Delta t_B$ normalized to γ_L as a function of the basic trapping frequency $\omega_T^{(E)}/\gamma_L$, for an experiment with $\gamma_L/\omega = .01$ and for an experiment with $\gamma_L/\omega = .005$. Measurements from both experiments are seen to agree within about 20% with the curve derived from the self-consistent calculations. Also, Figure 4.7 shows that for $\omega_T/\gamma_L \gg 1$, the self-consistent calculation approaches the prediction of O'Neil, as expected.

This verification of the applicability of trapping oscillation theory to standing waves in bounded plasmas is the second main result of this thesis. Also, since the nonlinear theory is based on the same collisionless Vlasov equation as the lin-

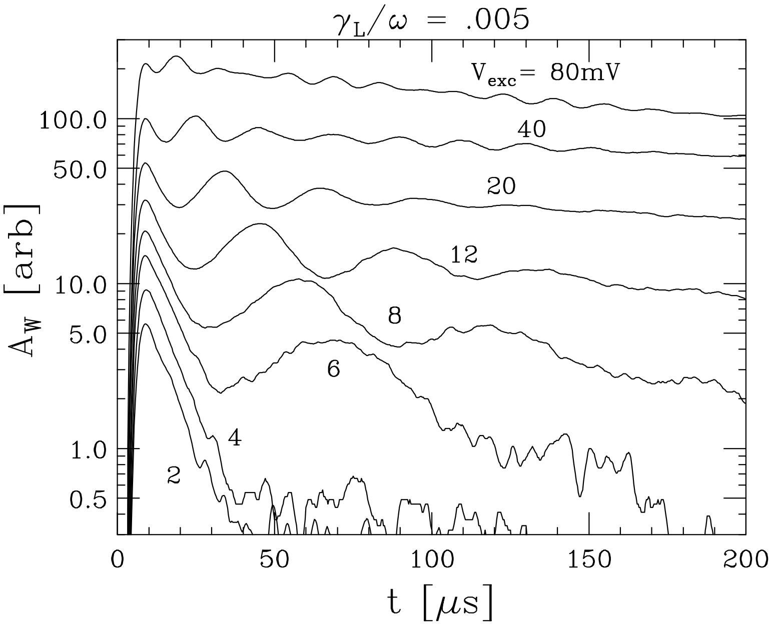

Figure 4.5: Recorded waveforms from a series of large amplitude wave decay experiments.

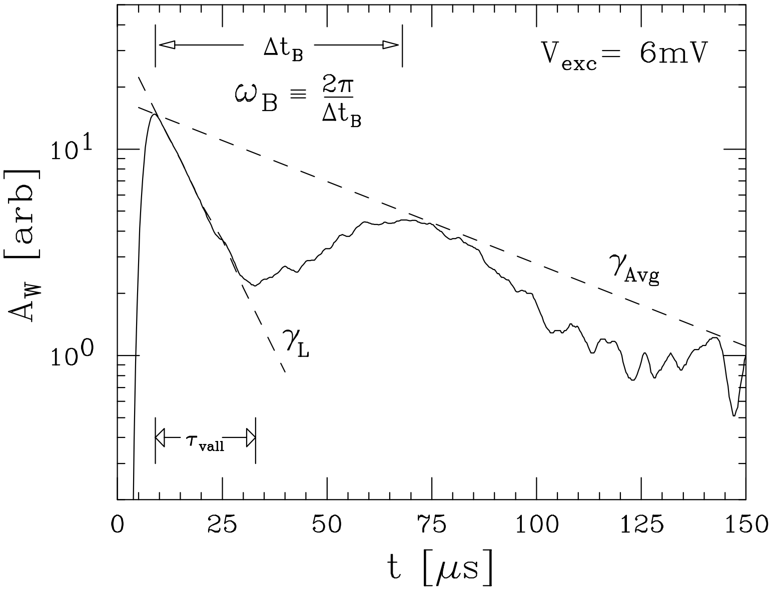

Figure 4.6: Definition of the amplitude bounce time Δt_B betweem wave excitation and the first amplitude peak, giving $\omega_B \equiv 2\pi/\Delta t_B$; and the amplitude valley time τ_{vall}; and the average damping rate γ_{avg}

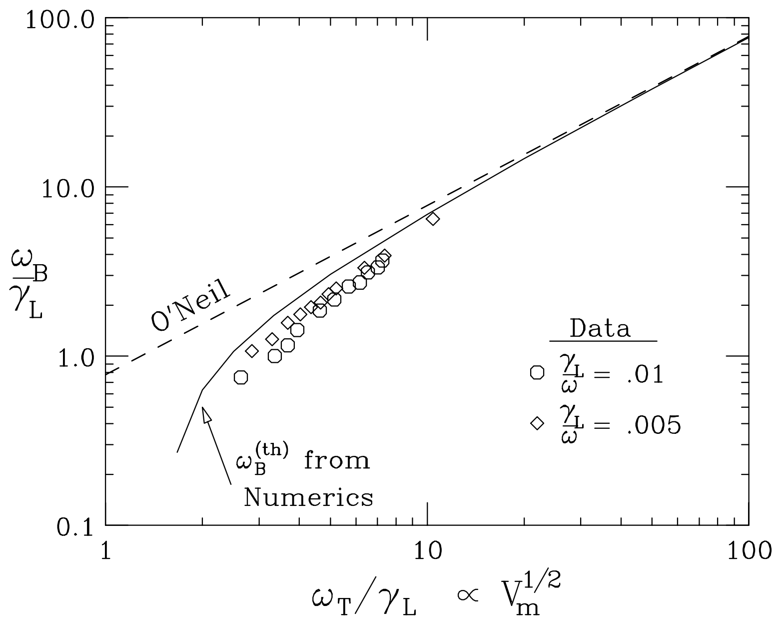

Figure 4.7: Measurement of ω_B with comparison to O'Neil and to the numerical self consistent caculations. The dashed line is the expected curve from the theory of O'Neil. The solid curve is from the self-consistent calculations.

ear theory, this agreement is further evidence that Landau damping is directly applicable to standing waves in our trapped pure electron plasmas.

4.3.2 Measurement of Valley Time (τ_{vall})

As a further check of the theory, we can look at other aspects of the theory that appear to be good indicators of the physics. One such indicator is the bounce time as used above. Another indicator is the time it takes to reach the first amplitude "valley" (τ_{vall}); this is the time it takes before the first particles start to become trapped.

The reciprocal valley time normalized to $\gamma_L/2\pi$ is plotted in Figure 4.8 for one set of data, along with the previous data for ω_T/γ_L for comparison, as well as the predictions from the numerical calculations. The valley time data shows excellent agreement with the numerics ($< 5\%$ difference); slightly better than the

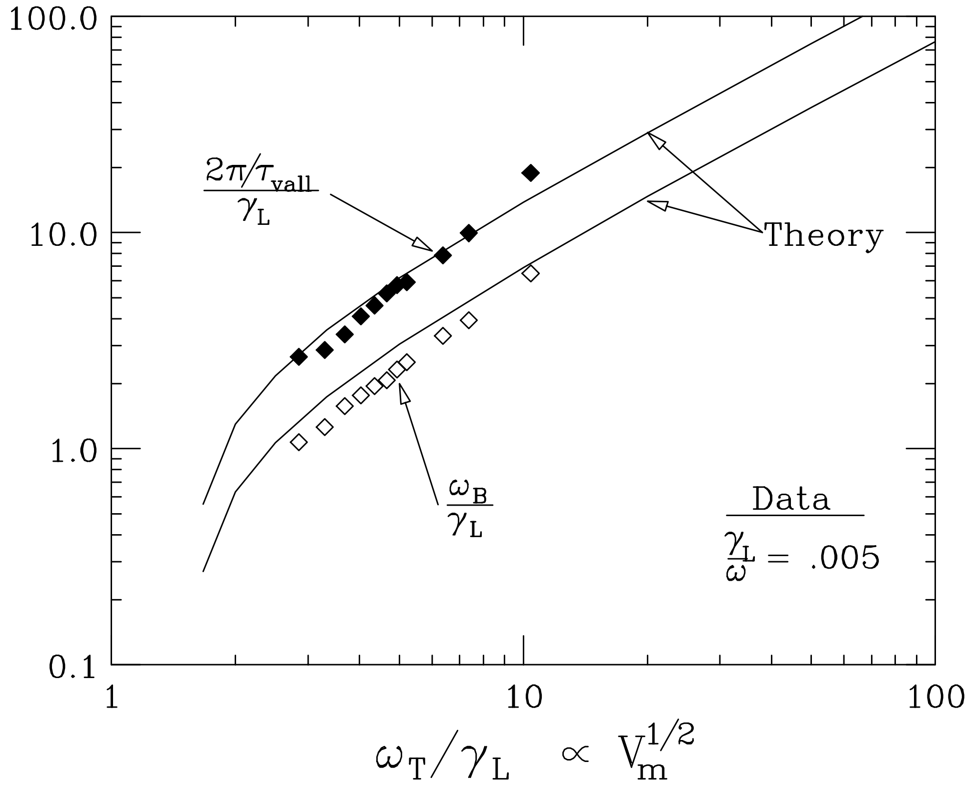

Figure 4.8: Measurement of ω_B and Valley time τ_{vall} with comparison to the self consistent caculations

comparison between the theory and ω_B. Presumably, this is because at early times, parasitic damping effects have had less effect on the wave amplitude and trapping process.

4.3.3 Measurement of Bounce and Valley Amplitudes

The oscillation rates (ω_B, $2\pi/\tau_{vall}$) are just half of the picture that the digitized data contains. The magnitude of the signal can also be checked. Figure 4.9 plots the bounce amplitude and valley amplitude (both normalized to the initial wave amplitude) versus ω_T/γ_L as obtained from Figure 4.5.

There are two main points we can get from this data. First, for the largest amplitudes ($\omega_T/\gamma_L \sim 10$), both data sets agree remarkably well with the numerical

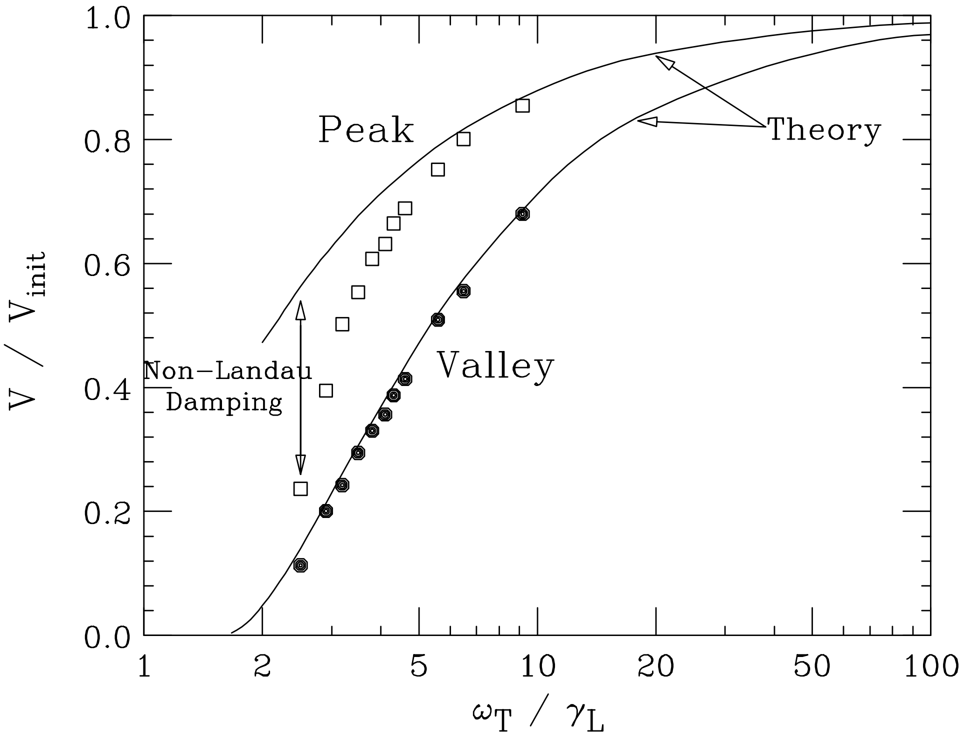

Figure 4.9: Measured amplitude of first peak and valley versus ω_T/γ_L.

calculations. However, as the amplitude gets smaller we observe that the bounce amplitude drops faster than the theory predicts. Second, although the bounce amplitude drops, the valley amplitude remains in agreement down to the lowest amplitudes.

This discrepancy is probably due to either residual damping from the resistive impedance of the measurement circuit, or due to Landau damping from collisional repopulation of the resonant electrons as described in Section 4.4. Since the valley time is shorter than the bounce time, there has been less time for either damping mechanism to cause a significant discrepancy. Moreover, the bounce amplitude, is lower than than the theory as would be predicted if there was a second damping mechanism present.

Another possible interpretation is de-trapping of the resonant electrons. If a significant number of electrons escape before giving their energy back to the wave, then the peak of the bounce oscillation would be lower. Currently, the experiments cannot distinguish the different contributions of these effects.

4.4 Collisional Repopulation

Section 3.4.3 (Figure 3.12) presented an experiment where collisions repopulated the resonant particles which were eliminated by hollowing. In this case, the collisions drive the velocity distribution back towards a Maxwellian, allowing Landau damping to continue. In the nonlinear bounce oscillations considered in this Chapter, trapped electrons form a plateau in the distribution function in the region near the phase velocity of the wave [52], effectively halting Landau damping. Again collisions will drive this modified velocity distribution back towards a Maxwellian, destroying the trapped particle plateau, and allowing Landau damping to proceed.

Zakharov and Karpman [53] were the first to investigate the effect of this collisional relaxation on the evolution of a large amplitude electron plasma wave, presuming the collisions to be with neutrals or ions. Sperling [54] later showed that the same effect occurs for electron-electron collisions, as occurs in our plasmas. More recently, Kaganovich [55] calculated the similar effect of particle trapping and collisions modifying the collisionless heating rate in a low pressure glow discharge plasma.

A nonlinear damping rate γ_{NL} is derived from an analysis of the kinetic equations with the assumption of weak Landau damping ($\omega_T \gg \gamma_L$) [53], giving

$$\frac{\gamma_{NL}}{\gamma_L} \approx 3.01 \left(\frac{\nu_{eff}}{\omega_T}\right)^3 \approx 3 \left(\frac{\nu_{eff}}{\gamma_L}\right)^3 \frac{1}{(\omega_T/\gamma_L)^3}. \tag{4.5}$$

Here the effective collision rate is given by $\nu_{eff} = (\bar{\omega}_{zt}^2\ \nu_{ee})^{\frac{1}{3}}$, where $\bar{\omega}_{zt} = \pi\bar{v}/L_p$ is

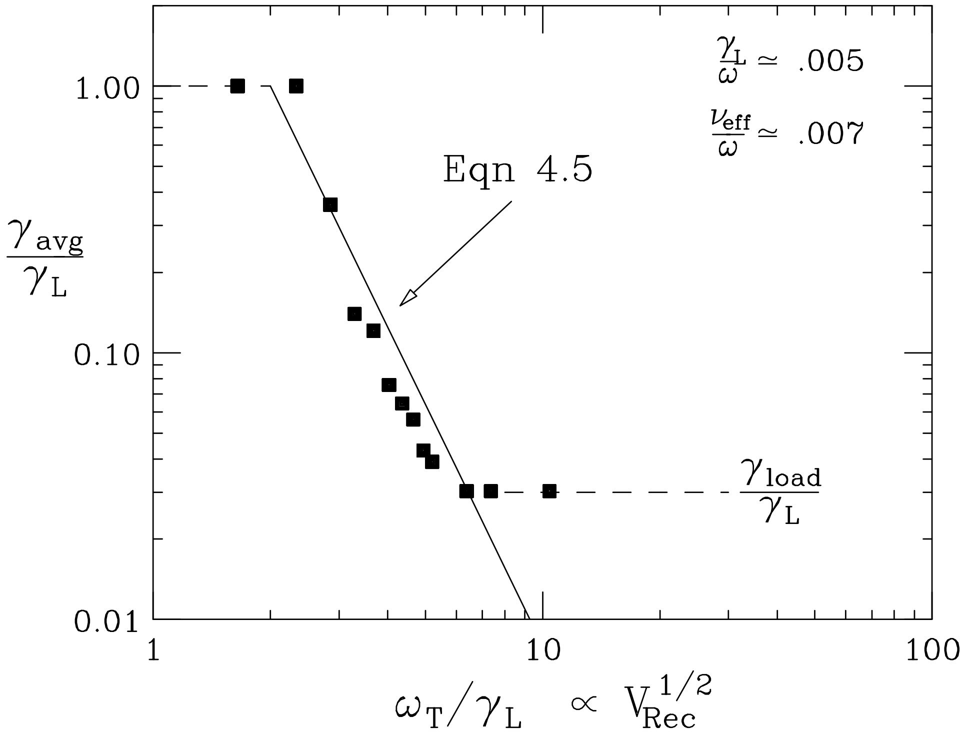

Figure 4.10: Comparison of measured average (nonlinear) damping rate (γ_{avg}) to the collisional repopulation of resonant particles predicted by Zakharov and Karpman.

the thermal electron axial transit (bounce) frequency.

From the experiments, the long-time (average) damping rate γ_{avg} is obtained from the amount of decay in 200μsec (see Figure 4.6) and is plotted in Figure 4.10 as the solid squares, along with the prediction from Equation 4.5.

For small amplitudes, γ_{avg} is the the same as the linear Landau rate and independent of amplitude. As the amplitude increases to where $\omega_T \gtrsim \gamma_L$, trapping oscillations appear and the damping rate decreases as predicted by Equation 4.5. At even larger amplitude, the damping rate again becomes independent of amplitude, determined by resistive dissipation in the detection circuit as indicated by γ_{load} in Figure 4.10.

Overall, we find close agreement with Equation 4.5 over the range 1 <

$\omega_T/\gamma_L < 10$, even though the theory is only valid for $\omega_T \gg \gamma_L$. The long-time damping is consistent with the dissipation of trapping oscillations due to collisional repopulation of resonant particles.

4.5 Measurement of Asymptotic BGK-like States

The time-asymptotic state of a large amplitude Landau damped wave has been predicted to be a BGK (Bernstein-Greene-Kruskal) equilibrium [44]. A BGK equilibrium is a particular velocity distribution which is self-consistent with a steady-state (undamped) large amplitude wave. No experimental observation of a large amplitude wave evolving to a BGK state has yet been made, but several numerical simulations have shown its development [45, 46, 47].

Experimentally, this issue has been complicated by the appearance of the "sideband instability" [6, 56]. The oscillations that develop at the sideband frequencies take energy from the main wave and further distort the velocity distribution. This makes a steady-state equilibrium between the wave and particles impossible.

In our finite-length electron column, there are no sideband waves possible because the T-G dispersion is fixed by the length of the system to discrete wavelengths parameterized by m_z, as previously shown in Figure 3.3. In practice, this should allow us to investigate the final state of a large amplitude wave without the complications discussed above.

The issue that complicates our experiments is the resistive damping due to the detection circuit. This extra damping causes a long-time dissipation of the wave potential, thus causing a reduced effective trapping frequency and a reduction of the "plateau" amplitude V_{plat} for any BGK state. Essentially, the predicted BGK amplitude is set by the initial amplitude of the wave (as seen in Figure 4.1);

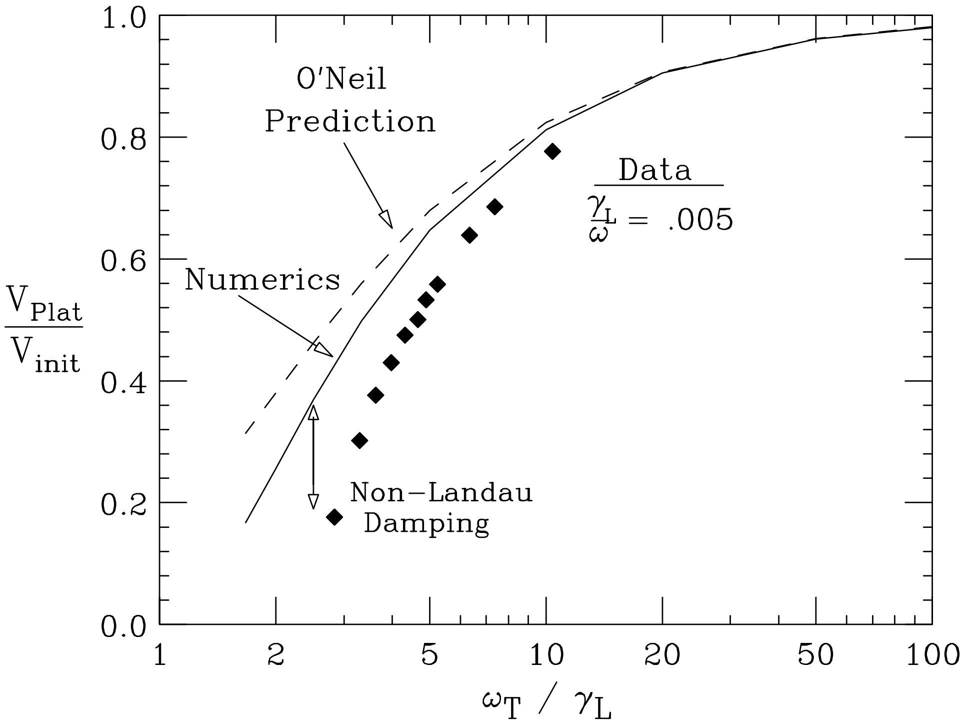

Figure 4.11: Measured plateau amplitude compared to theory, showing the effect of load damping at small ω_T/γ_L.

however, on times scales where resistive damping is important, the amplitude of the wave is no longer determined solely by the initial amplitude.

One way to obtain an estimate of the BGK amplitude is to use the average of bounce valley amplitude and the bounce oscillation amplitude. Calculations of this average from Figure 4.1 or Figure 4.2 show that this approximation differs from the long time amplitude by less than 5%. Figure 4.11 plots the average of the bounce and valley amplitudes versus ω_T/γ_L obtained from Figure 4.9, along with the predictions from the numerical calculations. Although there is decent agreement for waves with $\omega_T/\gamma_L \sim 10$, as the wave amplitude decreases, the disagreement increases, to as much as a factor of 2 for the smallest amplitudes ($\omega_T/\gamma_L \sim 2.5$).

The discrepancy between the data and the theory at small ω_T/γ_L in Figure 4.11 is the same as the discrepancy seen in Figure 4.9. Thus, the extra damping seen in the trapping oscillation experiments also causes the long time plateau amplitude to decrease and limits our ability to observe a pure BGK state. Further reduction of the resistive damping may allow an experimental test of the recent numerical simulations [45, 47].

Appendix A

Calculation of T-G mode dispersion

This Appendix shows the relevant equations used to derive the Trivelpiece-Gould (T-G) mode dispersion, as well as relate the measured voltages to the electric field in the plasma. This is used to calculate ω_T for large amplitude plasma waves.

The derivation of the T-G dispersion relation follows directly from their original paper [2]. The following is an outline of this procedure with all the relevant forumlas utilized in this thesis.

In the following we assume a cold plasma with uniform density plasma column, n_0 for $r < a$ and 0 for $a < r < b$, with a grounded conducting wall at b, confined by an infinite axial magnetic field (ie. $\omega_p/\omega_c \ll 1$), well below the "Brillouin" limit [1]. For this case the plasma dielectric tensor ε is given by

$$\varepsilon = \begin{bmatrix} 1 & 0 & 0 \\ 0 & 1 & 0 \\ 0 & 0 & 1 - \frac{\omega_p^2}{\omega^2} \end{bmatrix}. \tag{A.1}$$

The mode equation, $\nabla \cdot \varepsilon \cdot \nabla \delta\phi = 0$, becomes

$$\begin{aligned} &\nabla^2 \delta\phi - \left(\frac{\omega_p^2}{\omega^2}\right) \frac{\partial^2 \delta\phi}{\partial z^2} = 0 \quad && 0 < r < a \\ &\nabla^2 \delta\phi = 0 && a < r < b \end{aligned} \tag{A.2}$$

These equations are solved using cylindrical coordinates. The boundary conditions are that the potential $\delta\phi$ must by finite at $r = 0$, $\delta\phi$ is continuous at $r = a$, $-\nabla\delta\phi = \mathbf{E}$ is continuous at $r = a$, and $\delta\phi = 0$ at $r = b$, which is location the grounded conducting wall. Recognizing Bessel's equation, and defining $x \equiv k_z a\sqrt{\omega_p^2/\omega^2 - 1} \equiv k_\perp R_p$ the solution for $\delta\phi$, δE_z, and δE_r is written as

Inside: $0 < r < a$

$$\begin{aligned} \delta\phi(r,t) &= \frac{E_{z0}}{k_z}\, J_0\left(x\frac{r}{a}\right)\, \cos(k_z z) \\ \delta E_z(r,t) &= E_{z0}\, J_0\left(x\frac{r}{a}\right)\, \sin(k_z z) \\ \delta E_r(r,t) &= E_{z0}\frac{x}{k_z a}\, J_1\left(x\frac{r}{a}\right)\, \cos(k_z z) \end{aligned}$$

Outside: $a < r < b$

$$\begin{aligned} \delta\phi(r,t) &= b\, E_{rb} \ln(b/r)\, \cos(k_z z) \\ \delta E_z(r,t) &= bk_z\, E_{rb} \ln(b/r)\, \sin(k_z z) \\ \delta E_r(r,t) &= E_{rb}\, \frac{b}{r}\, \cos(k_z z) \end{aligned}$$

At the plasma-vacuum boundary: $r = a$

$$\begin{aligned} \delta E_z\ ; \qquad E_{z0} J_0(x) &= E_{rb}\, bk_z \ln(b/a) \\ E_{z0} &= E_r b\, \frac{k_z b \ln(b/n)}{J_0(x)} \qquad \text{(A.3)} \\ \delta E_r\ ; \quad E_{z0}\frac{x}{k_z a} J_1(x) &= E_{rb}\, \frac{b}{a} \\ E_{z0} &= E_{rb}\, \frac{k_z b}{x J_1(x)} \end{aligned}$$

Where E_{z0} is the value of the z component of the electric field evaluated at $z = 0$, and E_{rb} is the value of the radial component of the electric field evaluated at $r = b$ (ie. at the wall, see below). Eliminating the amplitudes using the above equations, we find the dispersion relation

$$x\ J_1(x)\ln(b/a) = J_0(x) \tag{A.4}$$

which gives us a relationship between ω, k_z, and the geometry of the plasma; with a equal to the plasma radius, b equal to the wall radius, and $x \equiv k_z a\sqrt{\omega_p^2/\omega^2 - 1}$ as before.

At the wall ($r = b$), we use Gauss' law to find a relationship between the induced image charges and the radial electric field E_{rb}.

$$\int_{surface} \mathbf{E} \cdot d\mathbf{A} = 4\pi\ Q_{\text{encl}}$$

$$2\pi b\ E_{rb} \int_{z_0}^{z_0+L_R} dz\ \cos(k_z z) = 4\pi Q_m$$

z_0 and L_R are the z location and length of the detection electrode, respectively.

Defining a new geometry function, $\hat{f}$,

$$\int_{z_0}^{z_0+L_R} dz\ \cos(k_z z) = \frac{1}{k_z}[\sin(k_z(z_0 + L_R)) - \sin(k_z z_0)] \equiv \frac{\hat{f}}{k_z}$$

we arrive at the relationship between the radial electric field at the wall and the induced charge on the detection electrode.

$$E_{rb} = \frac{2k_z Q_m}{b\hat{f}} \tag{A.5}$$

Further, since the current flowing through the detector feedback resistor is given by $I_{feed} = \omega Q_m$, and $V_m = I_f R_f$, where R_f is the value of the feedback resistor, then the measured voltage is $V_m = \omega R_f Q_m$. Solving for Q_m, and using Equation A.3 which relates E_{rb} and E_{z0}, we find:

$$E_{z0} = \frac{2}{\hat{f}} \frac{\ln(b/a)}{J_0(x)} \frac{k_z^2}{\omega} \frac{V_m}{R_f} \tag{A.6}$$

which is the desired formula relating the amplitude of the axial electric field of the wave to the measured voltage in the detector.

We can now use this to calculate ω_T for every measured plasma wave. From the definition of $\omega_T = \sqrt{eE_z k_z/m}$ we can write the trapping frequency (near r=0), as

$$\frac{\omega_T}{\omega_0}|_{r=0} = \sqrt{\frac{2}{\hat{f}} \frac{\ln(b/a)}{J_0(x)} \frac{e}{mv_\phi^3} \frac{V_m}{R_f}} \propto (V_m)^{1/2}. \tag{A.7}$$

We can further use Poisson's equation to solve for the density perturbation of the wave. Starting with

$$\nabla^2 \delta\phi = -4\pi e \delta n \tag{A.8}$$

plugging into Equation A.2 and using $\partial^2 \delta\phi/\partial z^2 = -k_z^2 \delta\phi$, we find

$$\delta n = \frac{1}{4\pi e} \frac{\omega_p^2}{\omega^2} k_z^2 \delta\phi. \tag{A.9}$$

Using $\omega_p^2 = \frac{4\pi e^2 n}{m}$, and recognizing that $\frac{ek_z^2\delta\phi}{m} = \omega_T^2$, and using Equation A.7 we can write

$$\frac{\delta n}{n} = \frac{\omega_T^2}{\omega^2} = \left(\frac{2}{\hat{f}} \frac{\ln(b/a)}{J_0(x)} \frac{e}{mv_\phi^3}\right) \frac{V_m}{R_f}. \tag{A.10}$$

This equation for $\delta n/n$ is used in Section 2.4 to measure and verify the amplitude calibration for the launched T-G modes.

References

[1] R.C. Davidson. *Theory of Nonneutral Plasmas.* Addison-Wesley, 1990.

[2] A.W. Trivelpiece and R.W. Gould. Space Charge Waves in Cylindrical Plasma Columns. *Journal of Applied Physics*, 30:1784, 1959.

[3] L.D. Landau. On the Vibrations of the Electronic Plasma. *J. Phys. (U.S.S.R.)*, 10:25, 1946.

[4] T. O'Neil. Collisionless Damping of Nonlinear Plasma Oscillations. *Phys. Fluids*, 8:2255, 1965.

[5] J.H. Malmberg and C.B. Wharton. Dispersion of Electron Plasma Waves. *Phys. Rev. Lett.*, 17:175, 1966.

[6] T.P. Starke, J.H. Malmberg. Sideband dispersion (plasma waves). *Phys. Rev. Lett.*, 37:505, 1976.

[7] *Non-Neutral Plasma Physics IV: Workshop on Non-Neutral Plasmas.* Edited by F. Anderegg, L. Schweikhard, and C.F. Driscoll. American Institute of Physics, 2002.

[8] J.M. Kriesel. *Experiments on Viscous and Asymmetry-Induced Transport in Magnetized, Pure Electron Plasmas.* PhD Thesis, University of California at San Diego, 1999.

[9] A.W. Hyatt. *Measurement of the Anisotropic Temperature Relaxation Rate in a Pure Electron Plasma* PhD Thesis, University of California at San Diego, 1988.

[10] D.L Eggleston, C.F. Driscoll, B.R. Beck, A.W. Hyatt, J.H. Malmberg. Parallel energy analyzer for pure electron plasma devices. *Phys. Fluids B*, 4:3429, 1992.

[11] B.R. Beck. *Measurement of the Magnetic and Temperature Dependence of the Electron-Electron Anisotropic Termperature Relaxation Rate* PhD Thesis, University of California at San Diego, 1990.

[12] B.P. Cluggish, J.R. Danielson, and C.F. Driscoll. Resonant particle heating of an electron plasma by oscillating sheaths. *Phys. Rev. Lett.*, 81:353, 1998.

[13] T.B. Mitchell. *Experiments on Electron Vortices in a Malmberg-Penning Trap.* PhD Thesis, University of California at San Diego, 1993.

[14] A.A. Kabantsev, C.F. Driscoll, T.J. Hilsabeck, T.M. O'Neil, J.H. Yu. Trapped-Particle asymmetry modes in single-species plasmas. *Phys. Rev. Lett.*, 87:225002, 2001.

[15] F. Anderegg, N. Shiga, J.R. Danielson, D.H.E. Dubin, and C.F. Driscoll. Thermally Excited Modes in a Pure Electron Plasma. Submitted to *Phys. Rev. Lett.* (Nov. 2001).

[16] J.D. Moody, C.F. Driscoll, Rarefaction waves, solitons, and holes in a pure electron plasma. *Phys. Plasmas*, 2:4482, 1995.

[17] B.M. Lamb and G.J. Morales. Ponderomotive effects in nonneutral plasmas. *Phys. Fluids*, 26:3488, 1983.

[18] S.C. Neu and G.J. Morales. Propagation of nonlinear pulses in a non-neutral plasma slab. *Phys. Plasmas*, 2:3033, 1995.

[19] J.G. Wang and M. Reiser. Longitudinal space-charge waves and instabilities in intense beams. *Phys. Plasmas*, 5:2064, 1998.

[20] J.G. Wang, H. Suk, D.X. Wang, and M. Reiser. Determination of the Geometry Factor for Longitudinal Perturbations in Space-Charge Dominated Beams. *Phys. Rev. Lett.*, 72:2029, 1994.

[21] H.S. Uhm. Space charge waves in a cylindrical waveguide with arbitrary wall impedance. *Phys. Fluids*, 25:690, 1982.

[22] P.J. Barrett, H.G. Jones, and R.N. Franklin. Dispersion of Electron Plasma Waves. *Plasma Physics*, 10:911, 1968.

[23] R.W. Landau and G. Schmidt. Oscillations of a Plasma Column. *Phys. Fluids*, 8:1890, 1963.

[24] A.W. Trivelpiece. *Slow-Wave Propagation in Plasma Waveguides.* San Francisco Press, Inc., 1967.

[25] J.K. Jennings, R.L. Spencer, K.C. Hansen. Numerical calculation of axisymmetric electrostatic modes for cold finite-length non-neutral plasmas. *Phys. Plasmas*, 2:2630, 1995.

[26] J.R. Danielson and C.F. Driscoll Measurement of plasma mode damping in pure electron plasmas. *Non-Neutral Plasma Physics III*, edited by J. J. Bollinger, et al., pages 214-219. American Institute of Physics, 1999.

[27] F.F. Chen. *Introduction to Plasma Physics and Controlled Fusion. Volume 1: Plasma Physics.* Plenum Press, New York, 1984

[28] B.D. Fried and S.D. Conte. *The Plasma Dispersion Function.* Academic Press, New York, 1961.

[29] C.J. McKinstrie, R.E. Giacone, and E.A. Startsev. Accurate formulas for the Landau damping rates of electronstatic waves. *Phys. Plasmas*, 6:463, 1999.

[30] F. Anderegg, N. Shiga, J.R. Danielson, and C.F. Driscoll. Thermal Excitation of Trivelpiece-Gould Modes in Pure Electron Plasmas. *Non-Neutral Plasma Physics IV*, edited by F. Anderegg, et al., pages 253-262. American Institute of Physics, 2002.

[31] J.R. Danielson, F. Anderegg, K.M. Rigg, and C.F. Driscoll. Landau Damping of Electron Plasma Waves in the Linear and Trapping Regimes. *Non-Neutral Plasma Physics IV*, edited by F. Anderegg, et al., pages 353-359. American Institute of Physics, 2002

[32] X. -P. Huang, C.F. Driscoll. Relaxation of 2D turbulence to a metaequilibrium near the minimum enstrophy state. *Phys. Rev. Lett.*, 72:2187, 1994.

[33] C.F. Driscoll. Observation of a $l = 1$ diocotron mode on a hollow electron column. *Phys. Rev. Lett.*, 64:645, 1990.

[34] X.-P. Huang. *Experimental Studies of Relaxation of Two-Dimensional Turbulence in Magnetized Electron Plasma Columns.* PhD Thesis, University of California at San Diego, 1993.

[35] S. A. Prasad. *Thermal Equilibria and Wave Properties of Finite Length Pure Electron Plasma Columns.* PhD Thesis, University of California at San Diego, 1981.

[36] M. Koepke, R.F. Ellis, R.P. Majeski, M.J. McCarrick. Experimental observation of bounce-resonance Landau damping in an axisymmetric mirror plasma. *Phys. Rev. Lett.*, 56:1256, 1986.

[37] R.L. Spencer, *Private Communication*, 1997.

[38] B.P. Cluggish. *Experiments on Asymmetry-Induced Particle Transport in Magnetized, Pure Electron Plasma Columns.* PhD Thesis, University of California at San Diego, 1995.

[39] A.J. Peurrung and J. Fajans. Nonneutral plasma shapes and edge profiles. *Phys. Fluids B*, 2:693, 1990.

[40] D.H.E. Dubin, T.M. O'Neil. Trapped nonneutral plasmas, liquids, and crystals (the thermal equilibrium states). *Rev. Mod. Phys.*, 71:87, 1999.

[41] D. Bohm and E.P. Gross. Theory of Plasma Oscillations. A. Origin of Medium-Like Behavior. *Phys. Rev.*, 75:1851, 1949.

[42] D. Bohm and E.P. Gross. Theory of Plasma Oscillations. B. Excitation and Damping of Oscillations. *Phys. Rev.*, 75:1864, 1949.

[43] D. Bohm and E.P. Gross. Effects of Plasma Boundaries in Plasma Oscillations. *Phys. Rev.*, 79:992, 1950.

[44] I.B. Bernstein, J. Greene, and M. Kruskal. Exact Nonlinear Plasma Oscillations. *Phys. Rev.*, 108:56, 1957.

[45] G. Brodin. New aspects on nonlinear Landau damping. (New Perspectives of Collective Effects. International Topical Conference on Plasma Physics, Trieste, Italy, 10-14 Nov. 1997). *Physica Scripta Volume T*, T75:204, 1998.

[46] G. Brodin. Nonlinear Landau damping. *Phys. Rev. Lett.*, 78:1263, 1997.

[47] M.B. Isichenko. Nonlinear Landau damping in collisionless plasma and inviscid fluid. *Phys. Rev. Lett.*, 78:2369, 1997.

[48] I.H. Oei and D.G. Swanson. Self-Consistent Finite Amplitude Wave Damping. *Phys. Fluids*, 15:2218, 1972.

[49] V.L. Bailey, Jr., J. Denavit. Nonlinear oscillations in a collisionless plasma. *Phys. Fluids*, 13:451, 1970.

[50] R. Sugihara and T. Kimimura. An asymptotic method for the Vlasov equation. III. Transition from amplitude oscillation to linear Landau damping. *J. Phys. Soc. Japan*, 33:206, 1972.

[51] D.L. Book. Landau Damping and Gorwth of Electrostatic Modes with Effects of Spatial Variation. *Phys. Fluids*, 10:198, 1967.

[52] R.Z. Sagdeev and A.A. Galeev, *Nonlinear Plasma Theory*, edited by T.M. O'Neil and D.L. Book. W.A. Benjamin, Inc. 1969.

[53] V.E. Zakharov and V.I. Karpman. On the Nonlinear Theory of the Damping of Plasma Waves. *Soviet Phys. J.E.T.P.*, 16:351, 1963.

[54] R.L. Sperling Electron Landau damping and electron collisions. *Phys. Fluids*, 21:514, 1978.

[55] I.D. Kaganovich. Effects of Collisions and Particle Trapping on Collisionless Heating. *Phys. Rev. Lett.*, 82:327, 1999.

[56] R.N. Franklin, R.R. MacKinlay, P.D. Edgley, D.N. Wall. Nonlinear behaviour of a finite amplitude electron plasma wave. III. The sideband instability. *Proceedings of the Royal Society of London, Series A (Mathematical and Physical Sciences)*, 360:229, 1978.